Universität Bonn
Physikalisches Institut

Molecular Orientation in Optical Polymer Films

von
Dirk Apitz

Post address:
Nussallee 12
53115 Bonn
Germany

BONN-IR-2006-04
Bonn University
April 2006
ISSN-0172-8741

Dieser Forschungsbericht wurde als Dissertation von der Mathematisch - Naturwissenschaftlichen Fakultät der Universität Bonn angenommen.

Diese Dissertation ist auf dem Hochschulschriftenserver der ULB Bonn
http://hss.ulb.uni-bonn.de/diss_online/ elektronisch publiziert.

1. Referent: Prof. Dr. K. Buse
2. Referent: Prof. Dr. P. M. Johansen

Tag der Promotion: 22. Dezember 2005

University of Bonn
Faculty of Mathematics and Natural Sciences
Institute of Physics

Molecular Orientation in Optical Polymer Films

Ph.D. Thesis
by
Dirk Apitz

In this thesis, orientation, dynamics, and electric conduction is investigated in films of various electro-optic polymers as functions of different parameters, such as the poling temperature and the chromophore concentration. The chromophore orientation distribution function is determined using electro-optic and dichroism measurements. The results are compared with those obtained by density-functional calculations and complementary wide-angle X-ray scattering. Time-resolved ellipsometry is used to record and analyze the dynamics of molecular orientation. Furthermore, dielectric spectroscopy is applied to investigate the influence of orientation on electronic conduction properties. The results of the analysis of the experimental data are compared with those obtained by Monte-Carlo simulations.

November 2005

Erscheinungsjahr: 2006

Contents

Chapter 1

Introduction

It occurs often that researchers discover effects or coherences in nature, which are either not exploited or even completely ignored for decades. Frequently, discoveries have a deep impact on science or they first lay at rest for some years before their application potential is recognized. Sometimes, however, the impact of research on our lives and on society leaves us stunned. Single findings can develop into an own scientific field with thousands of researchers feeding a billion-dollar industry, such as it is the case with several discoveries in genetics (immunology, virology, and cancer research). Another example is the use of light in technology. While the first coherent visible light source was realized in 1960 by Maiman [1], nowadays, we find laser diodes in every home. Displays of various kinds, optical methology, and optical material processing are together with information technologies booming areas in both, science and industry. All these fields require suitable optical materials for generation, transmission, handling, and storage of light. Some years ago, it has been recognized that polymers are promising: They are easy to handle and have many degrees of freedom for controlling their properties. Conducting organic materials, for example, are used for light emitting devices [2, 3], solar cells [4, 5], and photorefractive composites [6, 7, 8]. The linear electro-optic response, a change of the refractive index induced by an electric field, is stronger than in conventional crystalline materials. Furthermore, electro-optic modulation in polymers was shown to reach as far as the Terahertz range [9], far beyond what crystals are capable of due to the existence of phonons. However, even though the material properties in focus have been discovered many years ago, a broad exploitation has not yet occurred.

In order to use polymers, for many applications a specific structure has to be generated in the material, such as an optically written volume index grating or an electrically induced break of the inversion symmetry. In contrast to crystals, disordered materials exhibit a glass transition temperature causing dynamics to take place at all temperatures. When considered for technical application, however, temperature stability is often the most crucial characteristic feature. Usually, extrapolations of experiments at higher temperatures are performed to gain this kind of information. As an example, telecommunication devices are required to pass stability tests at 85 °C for

several weeks [10]. In addition to this experimental approach and also to understand polymer dynamics more profoundly, there is an ongoing effort to describe mathematically the dynamics of electro-optic dipolar molecules immersed in or covalently bound to a polymer matrix. Interactions of these chromophores with an external field [11] or the molecular surroundings of the matrix [12, 13] have been modeled to predict and explain polymer dynamics. However, so far dipole-dipole interaction has not been taken into account, even though a strong interaction is known from cooperative movements in polymers with high chromophore concentration [14]. It is not fully understood how chromophore-chromophore interaction and the dynamics in polymeric materials can be described efficiently in practice.

In many polymeric applications and processes, the conductivity of the material plays a central role. While a much broader interest is brought to highly conducting polymers, conduction is also important in nominally insulating polymers. Only if the electrical properties are completely understood and controlled, a more efficient way of processing insulating polymers is possible, such as for electro-optic applications. In order to exploit the electro-optic effect, for example, first it is required to break the inversion symmetry of the chromophore orientation by electric-field poling. It is an open and demanding question whether this orientation of the insulating material will enhance the electrical conductivity [15]. Strong orientation and high chromophore densities can even lead to liquid-crystalline phases of head-to-tail oriented chromophores [16], which may increase the conductivity significantly. This is of scientific interest, but also of practical relevance. In electro-optic devices AC and DC voltages are applied to such polymer films. Conductivity can cause unwanted drain currents that require excess power and generate heat. Furthermore, conductivity can even lead to a screening of the externally applied field and hence reduce the effective electro-optic coefficients [17].

This thesis with the title *Molecular Orientation in Optical Polymer Films* has to be seen as continuation and cross link between two lines of research activities: On the one hand, it has its origin in the tradition of a group at the Risø National Laboratory in Denmark, where cross feedback between fundamental optical experiments and the development of mathematical models were used to gain a deeper understanding of polymer dynamics [13]. This thesis intends to follow up those lines and to indulge into detailed investigation of dipole-dipole interactions in dye doped polymers. On the other hand, it is a collaboration and strong involvement with the polymer project of a research group at the university of Bonn, where mainly material properties of photoaddressable polymers and their technical applications, such as for integrated optics and a large area Fabry-Pérot modulator have been investigated [18]. In this tradition, this thesis intents to emphasize the fundamental research on the materials, which, with high and varying chromophore concentrations, show large dipole-dipole interaction and even crystallization.

In order to get a more profound understanding of the dipole-dipole interactions and the dynamics in polymers as well as of their impact on material properties, a variety of questions is asked and experiments are combined. For investigation of the dynamics and how they can be properly described, theoretical considerations are un-

dertaken using empirical functions. These are compared with the temporal behavior of the birefringence in polymer films recorded with a special ellipsometer. For more detailed information about orientation, the results of free beam electro-optic interferometry and linear dichroism measurements are combined and used to calculate the chromophore orientation distribution as a function of several poling temperatures and chromophore concentrations. In order to do so, the second order electro-optic coefficients and the angle-resolved absorption spectra in photoaddressable bis-azo copolymer thin films are measured. Density-functional calculations have been carried out on representative bis-azo monomers in several configurations and geometries to compare calculated absorption spectra with those obtained experimentally. Subsequently, the calculations on parallel and anti-parallel aligned dipole molecules (head-to-head and head-to-tail orientation) allow to study the influence of chromophore-chromophore interactions on absorption spectra and on the orientation. The partial order visible in the orientation distribution function of the chromophores is then confirmed with grazing incidence wide-angle X-ray scattering. Furthermore, the conductivity properties of polymers with a high density of bis-azo chromophores is analyzed. The influence of the chromophore orientation and of a transition to a liquid-crystalline phase are studied. Finally, charge carrier transport Monte-Carlo simulations are performed and compared with the experimentally obtained conductivity properties.

In order for the reader to understand easily the outline of the thesis, the following structure is chosen: After this introduction, in one chapter basic considerations are presented. Physical properties, such as photoisomerization, phase transition, electrical conductivity, mathematical descriptions of molecular orientation, and relaxation dynamics in polymers are introduced. The third chapter is dedicated to numerical calculations, where density functional calculations and Monte-Carlo transport simulations are explained. In the fourth chapter, the sample preparations and the experimental methods are described. Chapter five combines the presentation of the experimental results and the data analysis, such as curve fits and the calculation of distribution functions. In chapter six those results are interpreted and discussed. The main part of the thesis closes with a summery and an outlook.

Chapter 2

Basic considerations

2.1 Polymers

2.1.1 Structure

The materials used in this thesis contain azo benzene dye molecules (chromophores) either as a guest-host system (immersed in a containing polymer matrix [19]) or covalently bonded as side groups to the polymer main chain [20]. These molecules do not only show an electro-optic effect (if the molecular orientation is not inversion symmetric), but are also photosensitive. This means that a change of the refractive index can be induced by the application of an external electric field making use of the optical nonlinearity, as well as by the absorption of light [21], as it will be explained in the following.

A typical and very commonly used azo benzene dye molecule is 4-[N-Ethyl-N-(2-Hydroxyethyl)] Amino-4′-Nitroazobenzene (Disperse Red 1 or DR1), the structure of which is shown in Fig. 2.1. It consists of two polar end groups (an electron donator and an electron acceptor) connected by a delocalized, conducting π-electron system. This configuration creates a large permanent dipole moment. The chromophore molecules are in first approximation of a rod-like shape, which is why there is one dominating dipole component along the main axis of the molecule. It is convenient and justified to neglect the dipole moments perpendicular to it.

It has been discovered already in 1937 [22] that azo benzene can occur in two different geometries, a linear, stretched *trans* configuration and an angular *cis* configuration. The existence of these two isomeric configurations of the azo (NN) group are the origin of the photosensitivity. Figure 2.2 shows schematically those two geometries and the energy states of DR1. If the molecule absorbs a photon with a suitable energy it gets excited from a stable *trans* ground state $S_{0,\mathrm{t}}$ to a higher state $S_{1,\mathrm{t}}$, which can relax through a triplet state $T_{1,\mathrm{t}}$ into the ground state. The two triplet states of the *trans* and the *cis* configuration, however, are energetically very close. Therefore, there is a high probability of a transition between them. The excited *cis* triplet state $T_{1,\mathrm{c}}$ relaxes thermally into the *cis* ground state $S_{0,\mathrm{c}}$, which, again, is not stable and relaxes

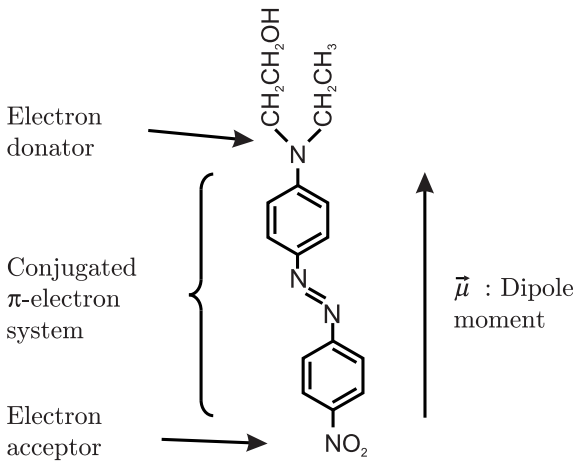

Figure 2.1: Schematic composition of Disperse Red 1 as an example for an azo dye.

further into the ground state of the *trans* configuration. Due to the shape differences of the two configurations, there is a non-vanishing probability that the final angular orientation of a molecule is after such a process not anymore the same as before [23].

The absorption probability of a photon is highest, if its polarization direction is parallel to the molecule's main axis and almost vanishes for a perpendicular orientation, because of the rod-like shape of the π-electron orbitals. Consequently, the repetition of several absorptions of linearly polarized photons and subsequent relaxations by an ensemble of chromophores results into an averaged overall orientation perpendicular to the direction of the light polarization. Thus, molecular orientation can be optically induced in such a polymer, which is therefore referred to as a photoaddressable material.

Strong interaction between the chromophores can furthermore entail cooperative movements, where the vibration of one chromophore effects the alignment of its neighbor chromophores, too [21]. Due to the geometrical and electrical anisotropy of the single molecules, an orientation also results into an anisotropy of the macroscopic absorption coefficient. This causes a change of the refractive index of the material (Kramers-Kronig relation). It shows dichroism and becomes birefringent. In the photoaddressable materials used, a birefringence of up to $\Delta n = 0.5$ could be verified [14, 24].

2.1.2 Phase transition

Disordered materials, such as polymers, do in the general case not solidify at a specific temperature, but undergo a continuous transition from a liquid or viscoelastic phase to a glassy or rubber-like phase over an extended region of temperatures when cooled down. Figure 2.3 shows schematically the behavior of the volume as a function of the temperature. The material possesses two different expansion coefficients and two different specific heat capacities, one each before and a distinct one after the transition.

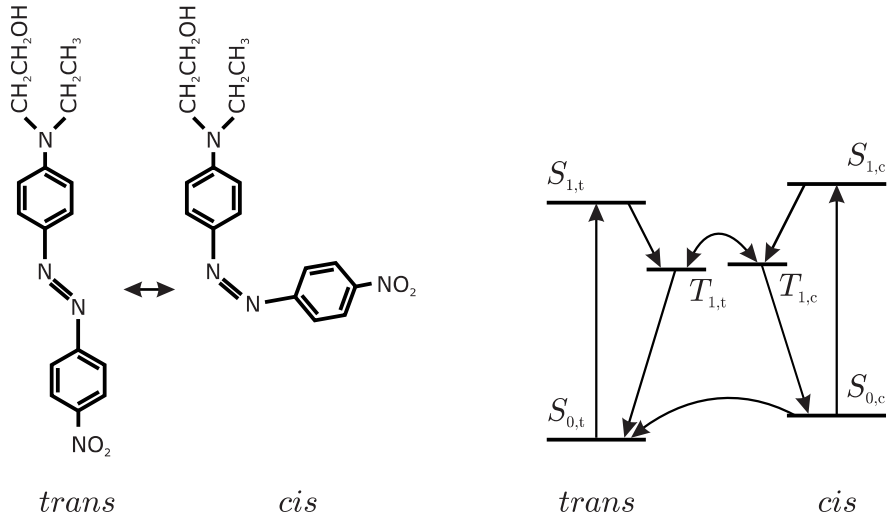

Figure 2.2: Photoisomerization of Disperse Red 1. Left: schematic representation of the molecule's *trans* and *cis* configuration. Right: simplified scheme of the energy states - ground and excited singlet states S_0 and S_1, as well as the excited triplet states T_1.

A possible definition of the glass transition temperature is where the two extrapolated dependences intersect. One way to measure this material property is differential scanning calorimetry (DSC), where the specific heat capacity is measured as a function of the temperature. However, this point is not always well defined, because the volume of a disordered material also depends on its history. If such a material is, for example, cooled down from the viscoelastic phase very slowly, then the material is much more compact in the glassy phase. The reason for this is that the polymer main and side chains have more time to move into and fill local free volumes in the material, which otherwise stay empty.

When polymeric materials undergo this phase transition under cooling, the polymer's main chains are no longer able to move, and their relaxation time diverges. In contrast to crystalline materials, not the first, but the second derivative of the volume to the temperature is discontinuous. This is why the glass transition is called a *second order* phase transition.

Besides the viscoelastic and glassy phase, polymers with a very high chromophore concentration can also be found in a *liquid crystalline* phase, if neighboring rod-like dipoles order in domains of, for example, head-to-tail orientation. These micro crystallites can, in fact, be very stable. Only by melting well above the glass transition temperature T_G and subsequent fast freezing [26, 27] or by solving in a suitable solvent and drying, the material can be transformed into the glassy phase again.

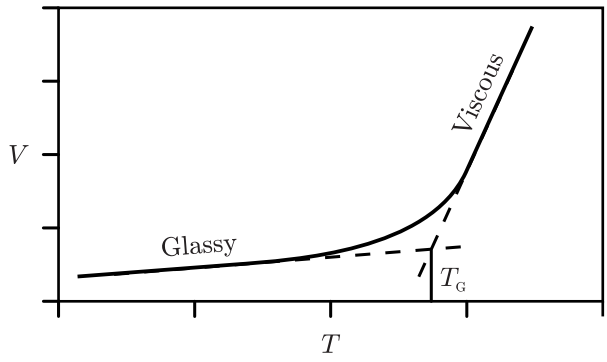

Figure 2.3: Schematic dependence of the volume V of a polymer as a function of temperature T in the region of the glass transition temperature T_G [25].

2.2 Orientation

2.2.1 Orientation distribution function

In isotropic (actually already non-inversion symmetric) materials, the second order nonlinear optical effects vanish. This can be easily illustrated with the example of the second order term of the polarization, for which the following expression can be given in the case of inversion symmetry

$$\vec{\mathcal{P}} = \epsilon_0 \hat{\chi}^{(2)} \vec{E}\vec{E} = \epsilon_0 (-\hat{\chi}^{(2)})(-\vec{E})(-\vec{E}) = -\vec{\mathcal{P}}, \tag{2.1}$$

where $\vec{\mathcal{P}}$ is the macroscopic polarization, ϵ_0 the electric permittivity of free space, and $\vec{E}$ the electric field. This equation is, of course, only correct, if also the hyperpolarizability tensor $\hat{\chi}^{(2)}$ vanishes. Thus, in order to enable a second order effect, such as the Pockels effect, the inversion symmetry of the orientation in the material has to be broken, such as by molecular orientation or by strong electric fields (e.g. in electric-field-induced second harmonic generation [28]).

For describing the orientation dynamics of nonlinear chromophores, a time-dependent orientation distribution function $g(\theta, \varphi, t)$ of the orientation solid angles (θ, φ) of chromophores immersed into a polymer matrix is introduced [11, 13] (see Fig. 2.4), with t being the time. Normalization requires for the integration over the entire solid angle that

$$\int_0^{2\pi} \int_0^{\pi} g(\theta, \varphi, t) \, \sin\theta \, \mathrm{d}\theta \, \mathrm{d}\varphi = 1. \tag{2.2}$$

In a disordered poled or nonpoled material, this distribution reduces to $g(\theta, t)$, because of having a rotational symmetry with the axis that points along the direction of the externally applied electric field $\vec{E}$. Furthermore, far below the glass transition temperature, the distribution can be considered to be independent of time.

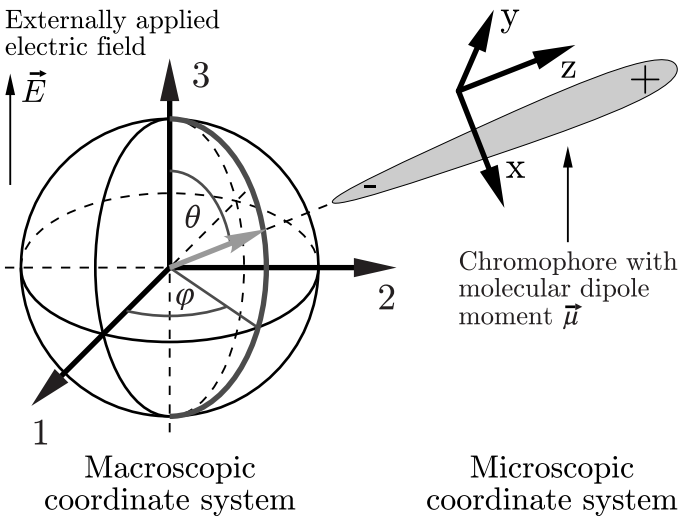

Figure 2.4: Angles in the macroscopic coordinate system.

Assuming a Maxwell-Boltzmann distribution function

$$g(\theta) = \frac{1}{4\pi} \exp\left(-\frac{U}{k_\mathrm{B}T}\right) = \frac{1}{4\pi} \exp\left(\frac{\mu_z^0 E_3}{k_\mathrm{B}T} \cos\theta\right) = \frac{1}{4\pi} \exp(\mathcal{E} \cos\theta), \tag{2.3}$$

with an interaction potential $U = -\vec{\mu} \cdot \vec{E}$ of the dipole moment $\vec{\mu}$ in the externally applied poling field $\vec{E}$, simple orientation distribution functions of the chromophores can be predicted. Here k_B is the Boltzmann constant, T the poling temperature, and $\mathcal{E}$ the dipole-external field interaction energy normalized by the thermal energy. This case, in which the interactions of the chromophores with the containing matrix, as well as dipole-dipole interactions between the chromophores are neglected, is referred to as the *oriented gas model* [11]. Figure 2.5 shows orientation distribution functions for three values of $\mathcal{E}$ using Eq. 2.3. It can be clearly seen that even strong poling fields do not manage to align all molecules. The distribution is still comparatively broad, though showing peaks at the solid angle's *north pole* ($\theta = 0$).

Because of the rotational symmetry, it is convenient to expand the distribution function in terms of Legendre polynomials P_j,

$$g(\theta) = \sum_{j=0}^{\infty} \frac{i_j}{i_0} \frac{2j+1}{2} P_j(\cos\theta), \tag{2.4}$$

where j is the counting index and i_j are the modified spherical Bessel functions

$$i_j(\mathcal{E}) = \frac{1}{2} \int_{-\pi}^{\pi} \exp(\mathcal{E} \cos\theta)\, P_j(\cos\theta)\, \mathrm{d}\cos\theta. \tag{2.5}$$

The order parameters $a_n = i_j/i_0$ can be introduced and obtained by averaging the j^{th}

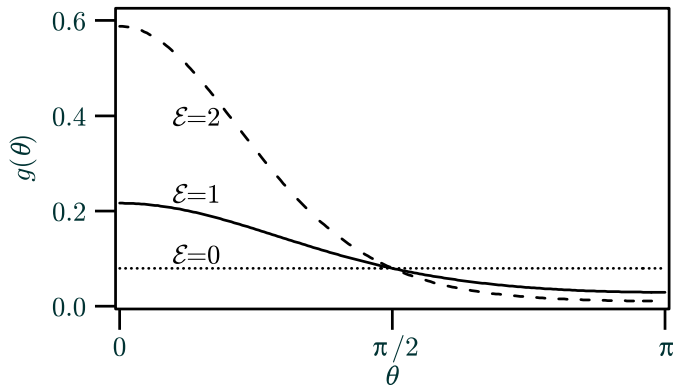

Figure 2.5: Normalized MAXWELL-BOLTZMANN orientation distribution function $g(\theta)$ as a function of the polar angle θ for three values of $\mathcal{E} = 0$ (dotted line), $\mathcal{E} = 1$ (solid line), and $\mathcal{E} = 2$ (dashed line), a parameter that quantifies the orientational energy of the chromophore in an electrical field normalized to the thermal energy.

LEGENDRE polynomials,

$$\begin{aligned} P_0(\cos\theta) &= 1, \\ P_1(\cos\theta) &= \cos\theta, \\ P_2(\cos\theta) &= \frac{1}{2}(3\cos^2\theta - 1), \\ P_3(\cos\theta) &= \frac{1}{2}(5\cos^3\theta - 3\cos\theta), \end{aligned} \tag{2.6}$$

over the entire solid angle with respect to the orientation of the chromophores,

$$\begin{aligned} a_j &= \int_0^{2\pi}\int_0^{\pi} P_j(\cos\theta)\, g(\theta)\, \sin\theta \,\mathrm{d}\theta \,\mathrm{d}\varphi \\ &=< P_j(\cos\theta) > . \end{aligned} \tag{2.7}$$

The first order parameter ranges from -1 to 1, and the second order parameter from -0.5 to 1. Often the first order parameter is just called *order parameter*, while the second one is called *alignment parameter*. To be able to also address higher orders, such as the third one, in this thesis they will be simply numbered.

2.2.2 First and third order parameter

Considering a glassy polymer with rod-like nonlinear optical molecules having a dominant hyperpolarizability along the z-axis of the molecule, β_{zzz}, and restricting the discussion to the linear electro-optic effect (POCKELS effect, second-order nonlinear electro-optic process), the induced microscopic polarization p_z^ω is given by

$$p_z^\omega = \beta_{zzz} E_z^\omega E_z^0, \tag{2.8}$$

where E_z^ω and E_z^0 are the electric field components of the light wave with the frequency ω and the externally applied DC field, respectively, both in the z-direction (see Fig. 2.4).

Integrating the orientation distribution of the molecular polarizations with the optical field parallel or perpendicular to the externally applied DC field leads to two components of the macroscopic polarization. From these relations the electro-optic susceptibility $\chi^{(2)}$ can be obtained as [11]

$$\chi_{333}^{(2)} = fN\beta_{zzz} < \cos^3\theta > \quad \text{and} \tag{2.9}$$

$$\chi_{333}^{(2)} = fN\beta_{zzz}\frac{1}{2}(< \cos\theta > - < \cos^3\theta >), \tag{2.10}$$

where N is the chromophore density and $<\cos\theta>$ the averaged cosine the orientation of all molecules. The local field factor f is added. Its use has been discussed controversially [13] and it has been described for regular crystal lattices by the LORENTZ law as $f = (\epsilon_{33} + 2)/3$. However, it also proved to be a good approximation for experimental systems consisting of dipolar molecules [29, 30].

Now, if birefringence is neglected, the POCKELS coefficients can be written as [31]

$$r = -\frac{2\chi^{(2)}}{n^4}, \tag{2.11}$$

where n is the refractive index. Contracting the first two indices and using Eqs. (2.6)-(2.10), one can calculate the order parameters from the measured POCKELS coefficients to be

$$a_1 = -\frac{n^4}{2fN\beta_{zzz}}(2r_{13} + r_{33}) \quad \text{and} \tag{2.12}$$

$$a_3 = \frac{n^4}{2fN\beta_{zzz}}(3r_{13} - r_{33}). \tag{2.13}$$

2.2.3 Second order parameter

Optical properties that are anisotropic, but inversion symmetric, such as birefringence or linear dichroism (anisotropic absorption), do not require a non-vanishing first order parameter. Considering a material with an anisotropic, rotational symmetric distribution $g(\theta, t)$ of anisotropically absorbing chromophores, a linearly polarized beam with the electric field vector parallel to the symmetry axis is consequently absorbed differently than one with a polarization perpendicular to it.

In the case of a polymer film (with the symmetry axis being the film normal 3-axis) tilted at an angle of γ_1 with respect to an incident laser beam, perpendicularly polarized light (with respect to the incident plane) has the electric field vector completely in the film plane and is subject to the absorption $A_\perp$ (see Fig. 2.6). Light polarized parallelly to the plane of incidence has the electric field vector at an internal angle of $\gamma_2 = \pi/2 - \arcsin(\sin\gamma_1/n)$ with respect to the film normal and experiences a different absorption $A_\parallel$ due to the out-of-plane component of the electric field vector. For

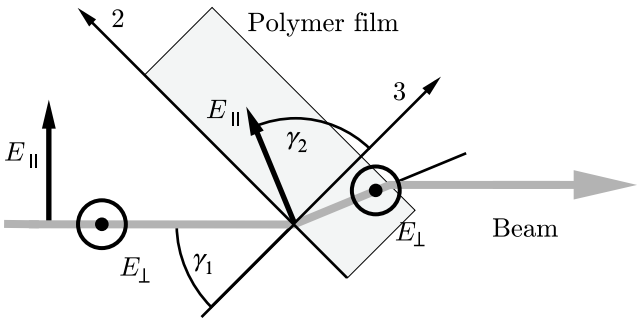

Figure 2.6: Transmission of differently polarized light through a film sample. This page is the plane of incidence. The film plane is perpendicular to it on top of the arrow marking the 2-direction.

the described constellation the second order parameter can be determined using the following expression for the dichroic ratio R [32]

$$R = \frac{A_\parallel}{A_\perp} = 1 + \frac{3\langle P_2\rangle}{(1-\langle P_2\rangle)n^2}\cos^2\gamma_2, \tag{2.14}$$

the derivation of which can be found in Ref. [33]. Typically, an anisotropic absorption most generally also requires an anisotropic refractive index. Thus, Eq. 2.14 is, of course, not strictly true, because the system is presumed to be uniaxially anisotropic. However, Johansson *et al.* gave a detailed calculation with the inclusion of the difference in the refractive indices, which makes the calculation incomparably more tedious, and he proved Eq. 2.14 to be applicable even for lipidic membranes [34, 35]. Estimating the deviation not to exceed a few percent, this first approximation gives the possibility for at least qualitative conclusions, which is the reason why, in this thesis, birefringence is neglected for simplicity. When restricting our experiments to a constant external angle $\gamma_1 = \pi/4$, the order parameter can, with Eqs. (2.6), (2.7), and (2.14), be reduced to the form

$$a_2 = \frac{2n^4(R-1)}{2n^4(R-1)+3}. \tag{2.15}$$

2.3 Conduction in polymers

An investigation of the complex conductivity $\sigma^*(\nu)$, of the complex permittivity or of the dielectric coefficient $\epsilon^*(\nu)$, respectively, as a function of the frequency ν of the applied electrical field $\vec{E}$ can give insights into structure and electrical properties on a molecular scale. Dielectric spectroscopy measures these properties.

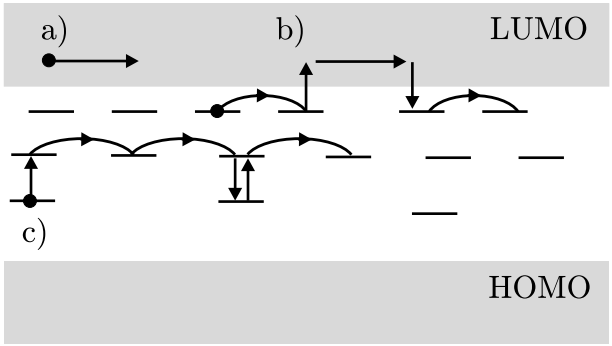

Figure 2.7: Charge carrier transport in polymers: a) free band conduction, b) charge carrier hopping using the conduction band c) thermally activated hopping.

2.3.1 Electronic conduction in disordered materials

In crystalline solid materials, conduction can be explained by considering the free electrons as propagating waves in a periodic lattice potential and disturbed by BRAGG reflection. The probability to find an electron at a certain location can be calculated using the SCHRÖDINGER equation. At BRAGG reflections, wavelike solutions to the SCHRÖDINGER equation do not exist. Energy bands (valence band and conduction band) and a band gap in between form with charge carriers delocalized over the entire crystal [36].

In disordered materials, however, there is no crystalline structure and thus no periodicity. Therefore, the band model can not be used for describing the electronic properties. However, it has been suggested to modify the model by introducing traps or localized sites energetically positioned within the band gap, which simulate the non-periodicity of the system [37].

In polymers, a certain periodicity can exist locally, for example one-dimensionally in the polymer main chain, where a description using the band model can make sense. In delocalized π-electron orbital systems, such as a simple benzene ring or conjugated polymers like the light emitting poly(*p*-phenylene vinylene) (PPV) [2], even conduction of delocalized (free) charges within the whole molecule is possible. Since the conduction properties of the entire material are not governed by something like a *conduction band* or a *valence band* the terms *highest occupied molecular orbital* (HOMO) and *lowest unoccupied molecular orbital* (LUMO) are used [38].

The major problem when modeling the conduction processes in disordered materials is to describe the distribution of traps. Several suggestions have been made for a distribution of the energy states, such as a GAUSSIAN distribution function [39]. Generally, however, an exponential distribution falling off from the HOMO is assumed. The classical band gap is replaced by a pseudo band gap with a low density of energy states. The energetic distance of a trap to the LUMO is referred to as the depth of the trap. The more disordered a material is, the bigger are the trap depths.

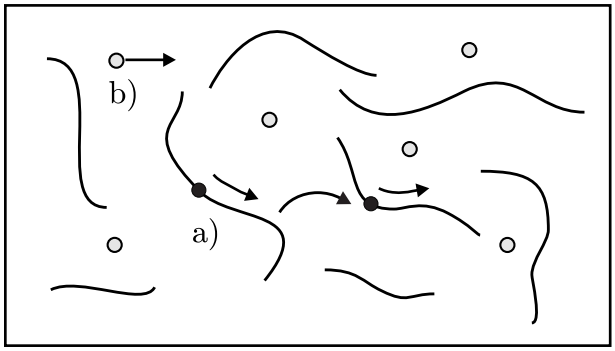

Figure 2.8: Charge carrier transport in polymers: a) inter-molecular electron or hole hopping, b) ion drift.

For conduction in polymers, one can distinguish between three types of charge carriers: electrons, holes, and ions. The most important conduction processes are schematically shown in Fig. 2.7 [40]. A free band conduction (Fig. 2.7a) like in metals requires a non-vanishing charge carrier density in the conduction band. This, however, is only given in conjugated polymers. Apart from the electron conduction displayed in Fig. 2.7a), also holes can contribute to the conduction in the HOMO. In electroluminescent polymers, they are even required for light emission, because they have to form excitons with the electrons to enable electron-hole recombination with the emission of photons.

In polymers, however, the conductivity is often dominated by the ability of the charge carriers to hop from one localized hopping site to another. Ions can use the local free volumes between the polymer chains. Electrons and holes hop (or tunnel) from one electron orbital in a molecule to another orbital or to an orbital in another molecule. Charge transport in these materials is, thus, governed by diffusive motion in contrast to Bloch electrons with well-defined wave vectors. These hopping processes can occur involving the conduction band (Fig. 2.7b) or by pure thermal activation (Fig. 2.7c) depending on the density of hopping sites.

The polymers investigated in this thesis are insulators. The DC conductivity is mainly governed by inter-molecular hopping processes shown in Fig. 2.8a). In these processes, the distance between the molecular orbitals plays a key role. Additionally, ionic conduction can occur, caused by ionic impurities from solvent residuals (Fig. 2.8b). These ions are not bound to the polymer molecules. However, their drift through the material is hindered by the polymer molecules. Thus, the ionic conductivity depends not only on the ion concentration, but also on the ability of the polymer side groups to move and to give way.

Conduction in *conjugated* polymers is basically governed by charge carrier hopping between delocalized π-electron orbitals that extend over the entire polymer back bone [2]. It is clear that basically film quality and orientation of molecular orbitals define the conduction properties of those polymers. As shown, e.g. in tetracene, the

conductivity along oriented polymer chains can be enhanced by several orders of magnitude with respect to the one perpendicular to them. However, conduction does not only play a key role in conjugated conducting polymers. The nature of conduction has also to be understood in all kinds of other polymers in order to optimize their fabrication and processing, such as chemical composition or poling procedures necessary to break the inversion symmetry in organic disordered electro-optic materials [8].

In insulating polymers, all sites are usually assumed to be localized [41]. However, photorefractive and nominally insulating electro-optic materials, such as the ones used in this thesis, contain a substantial amount of chromophores. There is no reason to assume that these molecules and their delocalized molecular orbitals do not participate as charge carrier hopping sites in conduction processes. These rod-like molecules can be assumed in a first approximation to be one-dimensional. The hopping distance to the next site in chromophore-doped systems and the number of hops required to cover a specific distance depend on the orientation distribution. Therefore, hopping probability and time of flight depend on the orientation distribution as well. This can be changed by poling, relaxation or a change into a liquid crystalline phase.

The electric conductivity of insulators in an externally applied AC field is mainly determined by the macroscopic polarization $\vec{\mathcal{P}}$ of the material, which again depends on the density and orientation of the permanent dipole moments $\vec{\mu}$ as well as on the molecular polarizability $\hat{\alpha}$. Even though the dominating dipoles in the materials used for this investigation are localized in covalently bonded polymer side groups, their orientation with respect to the polymer main chain, however, is flexible. Movements and reordering of both the main and the side chains can contribute to an overall change of the macroscopic polarization.

2.3.2 Dielectric relaxation

Dipolar relaxation has been described by Debye in 1912 [42]. Since then, dielectric spectroscopy has been proven useful to give deep insight into composition, structure, and dynamics of materials, and has been developed to a standard method in the field of material research. The principle is to apply an electric AC field to a sample and to measure the amplitude of the current as well as its phase. With this information, the complex permittivity ϵ^* and the complex conductivity σ^*, respectively, can be determined. Nowadays, frequency regions from 10^{-6} to 10^9 Hz in combination with temperatures between -180 to 400 °C are accessible. In this case, the term (dielectric) *relaxation* corresponds to resonances in the frequency space and is not to be confused with a relaxation (such as a decay) of a material from a perturbed state into an equilibrium.

The macroscopic polarization $\vec{\mathcal{P}}$ of a material as a function of the electric field $\vec{E}$ is given by

$$\vec{\mathcal{P}}(\nu) = \epsilon_0 \hat{\chi}(\nu) \vec{E}(\nu) = (\epsilon^*(\nu) - 1)\, \epsilon_0\, \vec{E}(\nu), \tag{2.16}$$

with ν being the frequency of the electric field. The permittivity

$$\epsilon^*(\nu) = \epsilon'(\nu) - i\epsilon''(\nu) \tag{2.17}$$

consists of a real part (ϵ') and an imaginary part (ϵ''). Both have, of course, a physical meaning. The quantity ϵ' determines how much energy can be reversibly accumulated in the material, while the imaginary part ϵ'' is proportional to the absorbed energy. Therefore, ϵ'' is referred to as the loss factor [43].

As already mentioned, the relative dielectric permittivity ϵ depends on the macroscopic polarizability of the material and thus on the dipole moment μ, the molecular polarizability, and the density N of the chromophores. The relation is given by the Debye equation [42]

$$\frac{\epsilon - 1}{\epsilon + 2} = \frac{\rho N_\mathrm{A}}{3\epsilon_0 M}\left(\alpha + \frac{\mu^2}{3k_\mathrm{B}T}\right) = \mathcal{P}_\mathrm{i} + \mathcal{P}_\mathrm{o}, \tag{2.18}$$

where ρ is the mass density of the material, N_A is Avogadro's constant, M the molar mass, and α the microscopic polarizability. The equation consists of an induced polarization part $\mathcal{P}_\mathrm{i} = \alpha\rho N_\mathrm{A}/3\epsilon_0 M$ and an oriented one, $\mathcal{P}_\mathrm{o} = \mu^2\rho N_\mathrm{A}/9\epsilon_0 M k_\mathrm{B}T$. Neglecting the atomic contribution to the polarizability, reduces Eq. 2.18 to the electronic polarization. This is applicable for very high frequencies and gives

$$\mathcal{P}_\mathrm{i} = \frac{\epsilon_\infty - 1}{\epsilon_\infty + 2}. \tag{2.19}$$

Setting $\rho N_\mathrm{A}/M$ equal to the chromophore density N, the expression

$$\frac{\epsilon - 1}{\epsilon + 2} - \frac{\epsilon_\infty - 1}{\epsilon_\infty + 2} = \frac{N\mu^2}{9\epsilon_0 k_\mathrm{B}T} \tag{2.20}$$

is derived. This equation is, of course, only a good approximation for gases. In order not to fail for liquids, Onsager added a term to describe an additional cavity field, which represents the polarization that originates from a reaction field acting on the dipoles that is a result of the electric displacement caused by its own presence. The extended version of the Onsager model delivers [44, 45, 46]

$$\frac{\epsilon - 1}{\epsilon + 2} - \frac{\epsilon_\infty - 1}{\epsilon_\infty + 2} = \frac{3\epsilon(\epsilon_\infty + 2)}{(2\epsilon + \epsilon_\infty)(\epsilon + 2)}\frac{N\mu^2}{9\epsilon_0 k_\mathrm{B}T}. \tag{2.21}$$

Figure 2.9 shows an ideal behavior of the permittivity as a function of frequency [43] for one relaxation process. Beyond both sides of the relaxation region, the real part ϵ' shows constant behavior. In between, however, it decreases with increasing frequency from the low frequency limit value ϵ'_l to the high frequency limit value ϵ'_∞ ($\nu \to \infty$) (Fig. 2.9 above). In this region, the imaginary part shows a characteristic relaxation peak with an amplitude $\Delta\epsilon''$ at the frequency ν_0 (Fig. 2.9 below). There have been several empirical functions offered for describing the spectrum of the permittivity, such

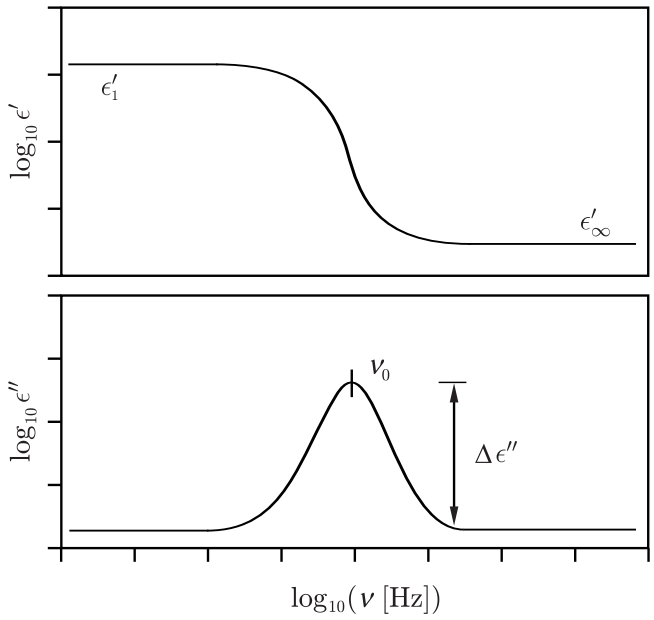

Figure 2.9: Frequency dependence of the real (ϵ') and the imaginary (ϵ'') part of the permittivity for one ideal dielectric relaxation, with the relaxation parameters ϵ'_1, ϵ'_∞, ν_0, and $\Delta\epsilon''$.

as the ones by Debye, by Cole and Cole, as well as by Davidson and Cole [43]. For polymers, most often the Havriliak-Negami function is used [47, 48]:

$$\epsilon^*(\nu) = \epsilon_\infty + \frac{\Delta\epsilon''}{[1 + (2\pi i\nu\tau_{\mathrm{HN}})^{\kappa_1}]^{\kappa_2}} \quad , \tag{2.22}$$

where κ_1 and κ_2 are two shape parameters defining the slopes of the peak. The response or relaxation time τ_{HN} is connected to the relaxation frequency ν_0 by the relation $\tau_{\mathrm{HN}} = (2\pi\,\nu_0)^{-1}$ and specifies the position of the maximum.

Figure 2.10i shows schematically a typical dielectric spectrum of a real polymer. Besides two relaxation peaks [49] centered at the frequencies ν_α and ν_β, a conduction contribution appears at low frequencies in the form of a straight line with the slope of -1. The two relaxation processes can be interpreted as resonances of the main polymer chain (primary or α-relaxation) and of the side groups (β- or Johari-Goldmann relaxation [50]). Exchanging side groups chemically or immersing plasticizing monomers generally changes the position and the broadness of *both* peaks, letting them sometimes only appear as shoulders of each other or of the conduction term in the graph. However, also polymers without side chains show a peak for a secondary relaxation. Therefore, one can also assign the two peaks to non-locally defined (α) and locally defined (β) relaxation processes. The dependence of the according relaxation times τ_α and τ_β on the temperature is shown schematically in Fig. 2.10*ii*. The faster β-relaxation is less temperature dependent than the α-relaxation, which diverges below the glass transition temperature T_{G} where the material freezes. Both processes merge together above the

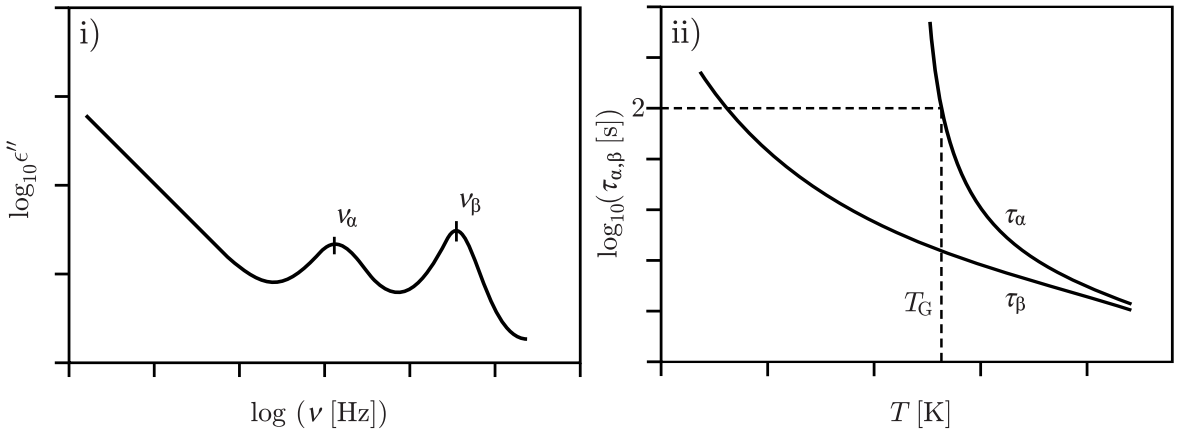

Figure 2.10: Schematically, Left: imaginary part of the permittivity ϵ'' with a conduction contribution (slope -1, at low frequencies) and two relaxation peaks at ν_α and ν_β, Right: relaxation times τ_α and τ_β as a function of temperature.

glass transition. Besides the DSC measurements mentioned in section 2.1.2, another possibility to define the glass transition temperature T_G is where the structural (α-) relaxation has a relaxation time of 100 s.

The conductivity σ^* can be directly deduced from the permittivity ϵ^* using the relation

$$\sigma^* = 2\pi i\nu\epsilon_0\epsilon^*(\nu). \tag{2.23}$$

The real part of the conductivity σ' and the imaginary part of the permittivity ϵ'' are linked to each other. Besides the peaks of the relaxation processes, a slope of -1 appears in the low frequency range of the permittivity, if the charge carrier conductivity asymptotically approaches a constant value being identical with the DC conductivity σ'_{DC}. In practice, however, such a value does not exist for all materials. In Fig. 2.11 both cases are shown. In materials with certain energetic distributions of traps, such a constant behavior can occur, if all the traps get filled with charge carriers at low frequencies and no more charge carriers can be captured, thus, leaving the charge carrier density constant.

Several microscopic models describe qualitatively the frequency dependence of the conductivity [51, 52, 53]. Assuming a conduction exclusively governed by hopping processes between hopping sites that follow the *random energy landscape model* [54], Dyre [55] provides the formula

$$\sigma^*(\nu, T) = \sigma'_{DC}(T)\left(\frac{2\pi i\nu\tau_t}{\ln(1+2\pi i\nu\tau_t)}\right) \quad , \tag{2.24}$$

for the complex AC conductivity σ^* based on the Continuous-Time-Random-Walk approximation [54], where σ_{DC} is the direct current value of the conductivity and τ_t is

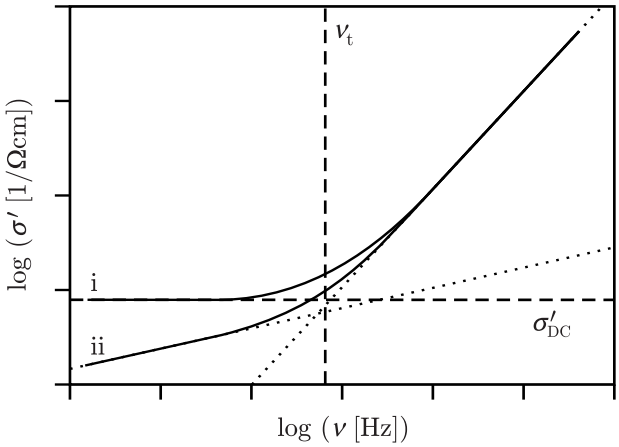

Figure 2.11: Typical conductivity spectra with (*i*) and without (*ii*) asymptotical approach to a constant value σ'_{DC}, while ν_{t} marks the transition frequency between the two regions of different behavior.

the time corresponding to a transition frequency ν_{t} between two regions of increment (slope +1) and leveling, when the largest energy barrier has been overcome [56].

Of course, the conductivity also depends on the temperature T. In materials with a high density of deep traps, such as in PMMA, poly(methyl methacrylate), a complete saturation of all traps with charge carriers does not occur. The conductivity does not show such a constant behavior for low frequencies. Even after a long drift time, additional charge carriers can still get caught in deep traps, constantly decreasing the number of carriers and therefore also the conductivity.

Since the number of free charge carriers in a material also depends on the temperature, temperature dependent measurements of the conductivity can reveal information about the conduction process and the material structure. Considering a simple diffusion model for the movement of the charge carriers [57, 58], the temperature dependence of the DC conductivity is described by the Vogel-Fulcher-Tammann (VFT) relation [59, 60, 61]:

$$\sigma'_{\mathrm{DC}}(T) \propto \exp\left(-\frac{E_{\mathrm{a},\,\sigma}}{k_{\mathrm{B}}(T - T_{\mathrm{V}})}\right) \quad , \tag{2.25}$$

where T is the absolute temperature and T_{V} the so-called Vogel temperature. At this temperature, the time constant for physical processes τ, such as structural relaxation, diverges adn the dynamics freeze. The activation energy $E_{\mathrm{a},\,\sigma}$ is the averaged energy needed in order to create free charge carriers.

Analysis of the spectra of the permittivity ϵ'' for different temperatures allows to gather information about properties of the ionic conduction processes. Because of the fact that the free ions are hindered by the polymer molecules in their motion through the material, a change in structure of the material will most likely result in a change of the ionic conductivity. The structural relaxation time τ_{HN} from Eq. 2.22 is correlated

with the temperature by [62]

$$\frac{1}{\tau_{\mathrm{HN}}} \propto \exp\left(-\frac{E_{\mathrm{a},\tau}}{k_{\mathrm{B}}T}\right) \quad , \tag{2.26}$$

following an ARRHENIUS behavior. Here $E_{\mathrm{a},\tau}$ is an activation energy for the relaxation. If the activation energies of the relaxation and of the conduction show a correlation in their behavior as a function of, for example, material, poling temperature or frequency, the dominating conduction process is limited by the movement of the side chains and can therefore assumed to be ionic.

2.4 Dynamics

If a system, that does not solidify by crystallization and remains in a disordered glassy state [63], is perturbed, then it shows strong non-exponential dynamics on the way to equilibrium. In this section, the question will be treated, how relaxation dynamics can be described correctly and which mathematical functions are suitable for the description.

Some theoretical models have been developed, such as the oriented gas model [11] or the DISSADO-HILL many-body relaxation model [64]. But they remain either too simple or are based on rather intuitive ideas. Thus, the dynamics is not yet fully understood. Nevertheless, it has become common to describe experimentally recorded, time-dependent responses $\phi(t)$ of relaxing systems, such as the optical birefringence, electric-field-induced second harmonic generation or photorefractive signals, by empirical functions, of which the most widely accepted is the KOHLRAUSCH-WILLIAMS-WATTS (KWW) stretched exponential function [65, 66, 67],

$$\phi_{\mathrm{K}}(t) = \phi_{\mathrm{K}}(\infty)\Big[1 - \exp[-(t/\tau_{\mathrm{K}})^{\xi_{\mathrm{K}}}]\Big]. \tag{2.27}$$

Here, ξ_{K} is the temperature dependent stretching exponent that can take values between zero and unity, τ_{K} is a characteristic relaxation time and the index K denotes the affiliation to the KWW function. Even though this function still behaves at long times approximately only like an exponential function, in many cases its universality seems striking. This feature has lead to attempts of explaining its physical origin [68].

However, dielectric experiments with polymers reveal the existence of two relaxation processes. Because of the existence of these two distinct relaxation processes it is investigated in this thesis, why in certain cases a single KWW function is *not* suitable for describing relaxation data, even though it is frequently used in literature.

Generally, a non-exponential relaxation behavior can be interpreted as a superposition of microscopic exponential decays in individual molecular environments and therefore with individual relaxation times τ [69],

$$\phi(t) = \phi(\infty)\left[1 - \int_0^\infty \exp(-t/\tau)\rho(\tau)d\tau\right]. \tag{2.28}$$

Macroscopically, the statistical ensemble of these relaxation times leads to a relaxation time distribution (RTD) $\rho(\tau)$. Normalization requires $\int_0^\infty \rho(\tau)d\tau = 1$. Setting Eq. 2.28 equal to Eq. 2.27, it becomes clear that the KWW function is not capable of describing *any* arbitrary RTD $\rho(\tau)$. This is only possible for distinct distributions $\rho_{\mathrm{K}}(\tau, \tau_{\mathrm{K}}, \xi_{\mathrm{K}})$, which then depend on the two parameters τ_{K} and ξ_{K} of the specific KWW function they describe. An explicit expression for such an RTD with $\xi_{\mathrm{K}} = 0.5$ has been given in Ref. [70],

$$\rho_{\mathrm{K}}(\tau, \tau_{\mathrm{K}}, 0.5) = \frac{1}{2\sqrt{\pi\tau\tau_{\mathrm{K}}}} \exp\Big(-\frac{\tau}{4\tau_{\mathrm{K}}}\Big). \tag{2.29}$$

This RTD is displayed as the long-dashed curve (a) in the upper graph of Fig. 2.12 with $\tau_{\mathrm{K}} = 1$ s. It consists of one peak and it falls monotonically off to zero on both sides. The curve is asymmetric on the logarithmic time scale approaching zero for long times more rapidly than for short times. It has been shown [70] that two relaxation functions with substantially different RTDs can both fit the same physical process equally well (Cole-Davidson function vs. KWW function). Nevertheless, it still depend on how much the real RTD of the physical system differs from the assumed one of the KWW fit function, whether a curve fit of the KWW relaxation function to specific experimental data will be of good quality.

The question is, in which cases the KWW function can be applied and what the limitations are. For a better understanding of the relation between a response $\phi(t)$ and its particular RTD, we consider Fig. 2.12 again. Besides the curve (a), the top graph shows four additional Gaussian distributions: with respect to the full-width-at-half-maximum, a narrow (dashed b), a broad (dash-dotted c), the sum of two narrow and well separated (thick solid d), and the sum of two broad and merging (dotted e) Gaussian functions on double-logarithmic scale. Due to the logarithmic time scale, normalization of these distribution functions with peaks in different regions of time results in amplitudes differing by orders of magnitude. Therefore, in order to be able to compare the distribution functions, they are displayed in the upper graph in Fig. 2.12 on double-logarithmic scale. Of course, Gaussian distributions differ from the KWW RTDs. However, their comparability (a relation between the broadness of the Gaussian and a value of ξ_{K}) has been shown by Xia [71]. Consequently, Gaussian distributions can be used to illustrate the central arguments in this thesis in an easier way.

The lower graph in Fig. 2.12 displays the response calculated using Eq. 2.28 together with the normalized distributions from the top graph. The one narrow Gaussian distribution (top graph, b) results in a decay still quite similar to a simple exponential function (short-dashed b and solid f, pair to the left). This means that even if the RTD does not consist of a single relaxation time (Dirac's delta distribution), it can still easily be described by a simple exponential relaxation, if it is just sufficiently narrow. The pair of curves in the center shows the relaxation with the one broad Gaussian RTD (dash-dotted c) and a stretched exponential behavior with $\xi = 0.45$ (solid g). So, in the case where the real RTD of a physical system is broad and consists of one peak, a stretched exponential function can describe the behavior.

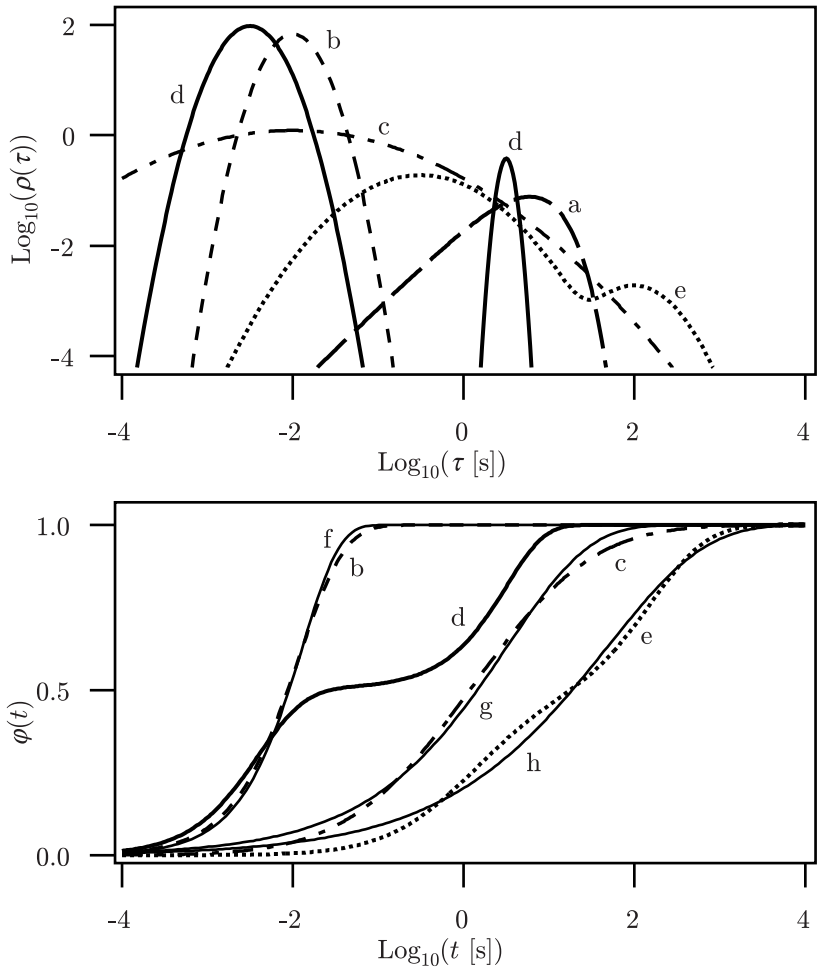

Figure 2.12: The top graph shows relaxation time distributions (RTDs) $\rho(\tau)$ on double-logarithmic scale. The long-dashed line represents the KWW RTD for $\tau_K = 1$ and $\xi_K = 0.5$ (a); a narrow GAUSSIAN (short-dashed, b), one broad GAUSSIAN (dash-dotted, c), a sum of two narrow (solid, d) and a sum of two broad (dotted, e) GAUSSIANS. Below, the according relaxations (along Eq. 2.28, using the same line types as above; b, c, and e) are shown together with (thin solid lines) a simple exponential relaxation (f), two KWW functions one with $\xi_K = 0.45$ (g) and one with $\xi_K = 0.38$ (h), and the relaxation with the RTD with the two narrow and separated peaks (wavelike thicker solid line, d).

To the right, the two curves display the relaxation with an RTD consisting of the two broad and merging peaks (dotted, e) and a KWW fit with $\xi = 0.38$ (solid h). This means that even if a relaxation behavior consists of several processes with more than one peak in the combined RTD, this example demonstrates that, as long as the peaks are low, broad and merging, it can still be seen as only one distribution, and the relaxation integral can become similar to a KWW function. However, the existence of two peaks in the RTD can be noticed already in the response by the dotted curve (e) wiggling more often around the KWW fit (h). Finally, the thick solid line shows the relaxation with the RTD of two narrow peaks (d). It results in a wavelike shape and it is clear that it cannot be represented with a single KWW function any more.

The temperature behavior of the stretching exponent ξ of the KWW function has been previously suggested in the form of a hyperbolic tangent [72]

$$\xi(T) = \xi_0 + \frac{1-\xi_0}{2}\left[1 - \tanh\left(\frac{A}{k_\mathrm{B}}\frac{T_0 - T}{T_0 T}\right)\right], \tag{2.30}$$

with T_0 a characteristic material temperature and ξ_0 the zero temperature value of $\xi(T{=}0)$.

Chapter 3

Numerical calculations

3.1 Density functional calculations

The specific visible light absorption behavior of molecules, such as the dependence on wavelength and polarizations, has its origin in the size and the shape of the electron orbitals. Consequently, the different shapes of azo benzene molecules in different isomeric (*trans* or *cis*) geometries also cause different absorption behaviors. Furthermore, electromagnetic intermolecular forces can provoke an approach of the molecules, such as in a liquid-crystalline phase, and a subsequent deformation. This deformation also results most likely in a change of the absorption. In order to interpret experimentally obtained absorption spectra, a comparison with numerically derived spectra can be helpful.

Density-functional calculations have been carried out on a simplified model molecule in various configurations shown in Fig. 3.1*i*-*v*. In those molecules, either both azo groups adopt a *trans* configuration (Fig. 3.1*i*) or only one azo group takes on a *trans* configuration (Fig. 3.1*iv* and 3.1*v*), while the other one takes on a non-planar *gauche* configuration. A local minimum in the energy of the geometry of the molecule, which corresponds to a planar *cis* type configuration has not been found. This type of *gauche* configuration will nevertheless be labeled *cis*. The optimizations of the geometry of the molecules have been carried out using the B3LYP exchange-correlation functional [73, 74], which is one of the most popular ones for molecular calculations. This is done in combination with a correlation-consistent basis set of polarized double-zeta quality [75]. It is known that good geometries for organic molecules can be achieved with this method. The Gaussian 03 program has been used for these calculations [74].

Based on the optimized geometry of the isolated *trans*,*trans* chromophore (both NN groups of the molecule are in a *trans* configuration, see Fig. 3.1*i*), several configurations have been created, in which two chromophore molecules are arranged in a relative parallel or anti-parallel orientation. This is done without further optimization of the molecule geometry. Calculations have been executed with distances of $d = 0.3$, 0.35, and 0.4 nm between the parallel molecular planes of the individual monomer molecules. These simple arrangements of chromophore dimers can be seen as a simple

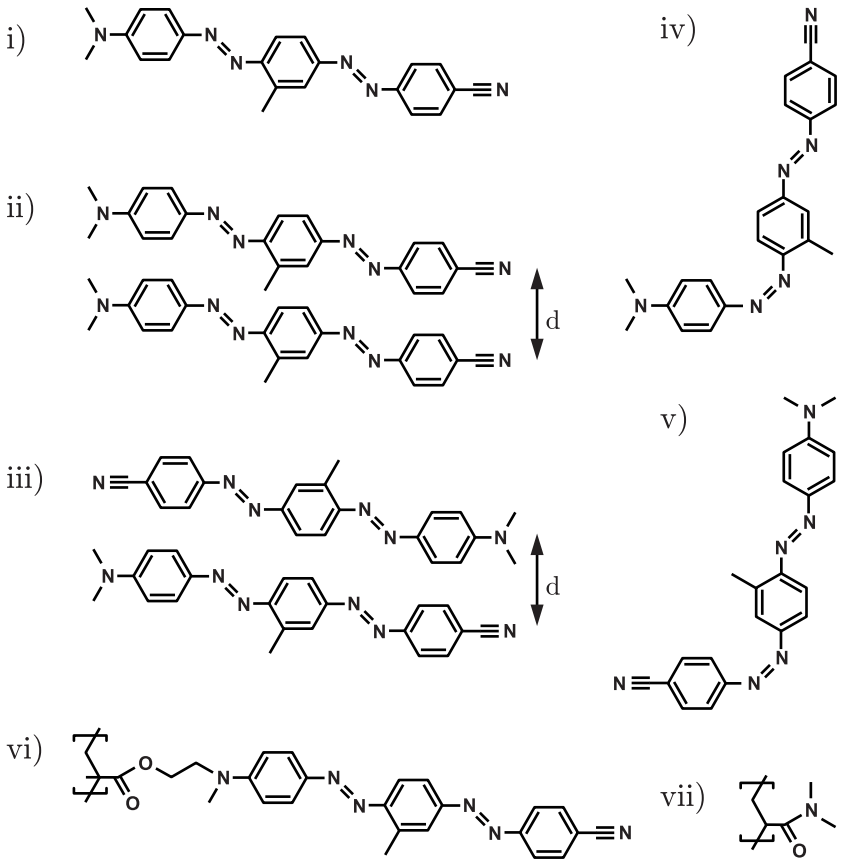

Figure 3.1: Chemical structures of chromophore monomers used for computation in a *trans*,*trans* configuration (i), schematic drawings of their relative positions with the distance d between molecules lying in parallel planes, with dipoles in parallel (ii) and anti-parallel (iii) orientation, in a *cis*,*trans* configuration (iv) and in a *trans*,*cis* configuration (v), and for comparison schematic drawings of the polymers used for the experiments (statistical compositions of the units vi and vii).

model in order to investigate the influence of chromophore-chromophore interactions on the optical properties.

With this set of monomer and dimer geometries, the optical absorption spectrum has been obtained using density-functional calculations with an exchange-correlation functional. Vertical electronic excitation energies and corresponding intensities are calculated within time-dependent density-functional theory (TD-DFT) [76, 77] as implemented into the Amsterdam Density Functional program (ADF) [78, 79]. The quality of the results is limited by two major approximations: the quality of the one-electron basis set employed on one hand and the choice of the exchange-correlation functional on the other hand. Here, an exchange-correlation potential and kernel is used, because of the local density approximation (LDA). This is done in combination with a basis set of polarized double-zeta quality (DZP basis set). With the chosen level of computation and the kind of larger molecules studied, the errors are expected to not to exceed approximately 0.5 eV for valence excitations. In order to obtain a higher accuracy of the results, a more sophisticated approach could be used at the cost of higher demands in computational resources.

3.2 MONTE-CARLO transport simulation

In the past, there have been attempts to mathematically describe and numerically simulate the conduction in insulating disordered materials with isolated localized sites and traps, as well as in conjugated polymers with extended π-electron orbitals. For simulation of conduction behavior it has proved valuable to apply random walk MONTE-CARLO simulations. Here, we are in particular interested in the influence of the orientation of rod-like chromophores serving as hopping sites.

In order to describe the orientation of the chromophores, again, the orientation distribution function $g(\theta, \varphi, t)$ as introduced in section 2.2.1 is adopted as well as the above-mentioned oriented gas model. The normalized interaction energy $\mathcal{E}$ (Eq. 2.3) can usually not exceed a value of about unity in disordered systems, due to the limits of the field strengths applicable and the influence of thermal agitation $k_\mathrm{B}T$. However, $\mathcal{E}$ can be used as a parameter for describing the degree of orientation, which increases far beyond that limit when undergoing a transition into a liquid crystalline phase. Thus, $\mathcal{E}$ is referred to as the orientation degree, in a wider range of values and meanings.

For simulation, the conduction properties, the polymer film is described three-dimensionally with periodic boundary conditions in 1- and 2-direction, while the 3-direction defines the film normal (see also Fig. 2.4). Chromophores are placed at random position and with a specific orientation. While the azimuthal angles φ are completely random, the polar angles θ follow a distribution according to those displayed in Fig. 2.5. However, the orientation of neighboring molecules does not have any correlation. For each chromophore i, the hopping direction $\overrightarrow{l_{ij}}$ and the effective minimal distances $\|\overrightarrow{l_{ij}}\| = l_{ij}$ to neighboring sites j is calculated. Figure 3.2 shows the three possibilities for shortest distances: (a) between the ends of two sites, (b) between the

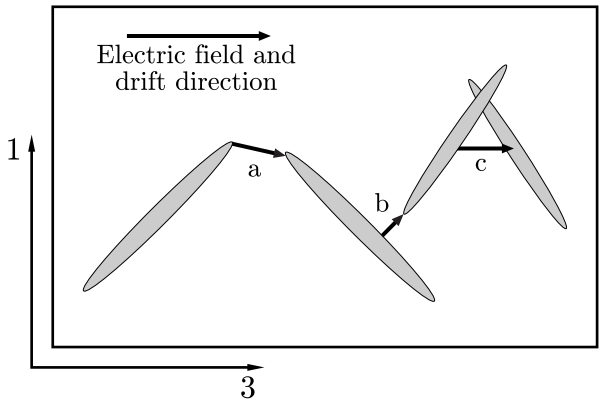

Figure 3.2: Schematic jump geometries between delocalized hopping sites. Shortest distances can occur (a) between the ends of two chromophores, (b) between an end and a middle part, and (c) between skew chromophores.

end of one and a middle part of another site, and (c) between two middle parts in a general skew geometry. Then the hopping probabilities to the adjacent transport sites are calculated. Generally, hopping rates W over a distance l can be defined as [68]

$$W(l) = u \ \exp(-2l/r_0), \tag{3.1}$$

where u is an l-independent prefactor and r_0 the localization radius of the electron wave function. In the case with an electric field $\vec{E}$ applied across the film, the probability to hop along the field is increased, the one for moving against the field is decreased, and those to hop perpendicular (in the film plane) is constant. This is due to the energy barrier being raised or lowered, but can also be modeled in the equation by increasing or decreasing the effective distance l_{ij} as a function of the applied field E and the hopping direction $\overrightarrow{l_{ij}}$. Therefore, an empirical factor

$$d(\overrightarrow{l_{\mathrm{ij}}}, E) = \exp\left(- D(E)\frac{l_{\mathrm{ij,3}}}{l_{\mathrm{ij}}}\right) \tag{3.2}$$

is proposed, which fulfills precisely these requirements and has to be a function of the applied field E via the prefactor D. This is only one possible way to describe the dependence caused by higher energy barriers or longer tunneling distances. In our case, the hopping probability is consequently set to

$$W_{\mathrm{ij}}(\overrightarrow{l_{\mathrm{ij}}}, E) = u \ \exp\left(- 2d(\overrightarrow{l_{\mathrm{ij}}}, E)\frac{l_{\mathrm{ij}}}{r_0}\right). \tag{3.3}$$

The parameters that can be varied are the chromophore density ρ, the orientation degree $\mathcal{E}$, and the driving field D.

For the simulation, electrons are placed on the hopping sites closest to the bottom electrode. Then, a random walk simulation is started. The drift of the charge carriers

caused by the externally applied field results in a time-dependent current. Each step of the random walk corresponds to a time unit δt in arbitrary units. The total current at each time t is given by [80]:

$$I(t) = \frac{\delta}{\delta t} \sum_{Z=0}^{d} \rho(Z) + \frac{1}{d} \frac{\delta}{\delta t} \sum_{Z=0}^{d} Z\rho(Z), \tag{3.4}$$

where Z is the position in 3-direction and $\rho(z)$ is the charge density integrated in the 1- and 2-directions. The first term of Eq. 3.4 gives the conduction current, whereas the second term corresponds to the displacement current, for which detailed investigation has shown that it is a small correction to the conduction term [81]. As the charge carriers move, the injected Delta-distribution centered at the bottom electrode disperses and typically propagates in a GAUSSIAN package across the film, if an electric field is applied. The mean transit time t_{T} can be defined as the time when the peak of the spatial GAUSSIAN charge distribution has reached the other electrode, that is when half of the charges have accumulated at the other electrode. The transit time is related to the effective charge carrier mobility m and the external field E via the relation

$$m = \frac{v}{E} = dt_{\mathrm{T}}E, \tag{3.5}$$

where v is the velocity, and this is how m is derived in time-of-flight measurements. The mobility, again, is linked to the conductivity σ by the equation $\sigma = qmN$, where q is the charge and N the carrier density.

Chapter 4

Experimental methods

4.1 Materials and samples

For the various experiments, two types of materials and sample geometries are used. For the investigation of the polymer dynamics in the ellipsometry measurements, drop-casted (thick) guest-host polymer films are applied. The samples investigated in all other experiments consist of spin-coated thin film copolymers.

4.1.1 Guest-host thick films

The azo benzene dye Disperse Red 1 (DR1, see Fig. 2.1), is mixed with the material of a matrix of poly(methyl methacrylate) (PMMA), as well as a plasticizer ethylcarbozole (ECZ), with wich one is able to tune the glass transition temperature. The three materials used consist of 80% PMMA and then additionally either (material 1) 15% DR1 and 5% ECZ, (material 2) 5% DR1 and 15% ECZ, or (material 3) 20%DR1, respectively. The three mixtures in the form of powder are solved in tetrahydrofuran (THF) using a supersonic bath, after which the solvent is evaporated. The samples are produced by drop casting the polymer between glass substrates using glass beads of 100 μm diameter as spacers and a heating plate. The substrates are each coated with a layer of indium tin oxide (ITO) partly etched in order to obtain stripe electrodes from one side to an area in the middle.

4.1.2 Copolymer thin films

The polymers investigated are one homopolymer and four copolymers, the synthesis of which can be found in Refs. [82] and [83]. The homopolymer consists of 100 % of the unit shown in Fig. 4.1*i*, which is functionalized with a side-chain bis-azo chromophore and has an averaged molar mass of 11500. The copolymers are statistically built up by the two monomer units shown in Fig. 4.1*i* and Fig. 4.1*ii*. Copolymers with 20, 40, 60 and 80 mol% of unit *i* are polymerized with averaged molar masses of 10500, 12700, 13300, and 12500, respectively. The chromophore shown in Fig. 4.1*i*

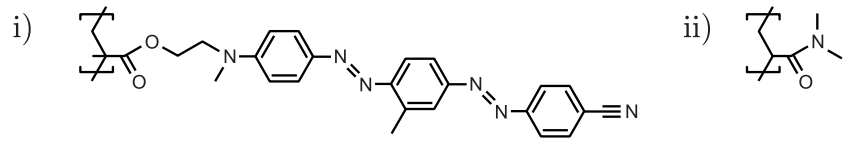

Figure 4.1: Chemical structure of the monomer units of the investigated photoaddressable bis-azo polymers used for the thin films.

has an approximate dipole moment of $\mu = 7$ D (1 Debye $= 3.336 \times 10^{-30}$ Cm) as estimated by density-functional calculations using the chromophore shown in Fig. 3.1*i*, and a hyperpolarizability $\beta_{zzz} = 8.36 \times 10^{-38}$ Vm^4 measured using Hyper-Rayleigh-Scattering (SHG, $\lambda = 1500$ nm $\rightarrow$ 750 nm, where λ is the wavelength of the light) [84]. The chromophore density has been estimated to be $N = 1.575 \times 10^{27}$ m^{-3} for the polymer with 100 % chromophore content. For the series of the electro-optic and absorption measurements as a function of the poling temperature a fraction of the 100%-material with a higher glass transition temperature (120 °C) is used [85].

The polymers are dissolved in cyclopentanone with a concentration of 100 mg/ml and spin coated in different film thicknesses onto ITO coated glass substrates of 25 × 25 mm size. The rotation speed is of the order of 3000 rpm and is varied in order to obtain several film thicknesses. The films are dried in a vacuum oven at 80 °C for several hours. Typical film thicknesses are 0.5 - 2.0 µm measured using a profilometer (Dektak). For the investigation of the conduction properties (see section 4.6), it was tried to reach larger film thickness in order to match capacity requirements for the highest accuracy of the dielectric spectrometer (10^{-9} F for the frequency region used of $10^{-3} - 10^{7}$ Hz). Unfortunately, the films show crinkles up from 2 µm thickness.

The films with 100 % chromophore content are corona poled [86] at 84, 94, 99, 102, 104, 109, 114, and 124 °C with an electric potential of +5 kV applied perpendicular to the film plane by a corona tip positioned 7 mm above the film plane, while the polymer films with different chromophore concentrations are each corona poled at their individual, previously determined, optimal poling temperature with respect to highest Pockels coefficients (see Table 4.1).

Finally, the sample is covered by a top electrode. For the dielectric measurements to each sample, an adhesive conductive pad with 3 mm diameter is attached. The diameter of the adhesive conductive pads is chosen to match the above mentioned capacitance requirements of the dielectric spectrometer in order to achieve high measurement accuracy. Other types of electrodes have been tried out, but have proved to be disadvantageous: (1) A sputtered gold electrode penetrates into microscopic surface defects, which then dominate the current or may short-circuit the sandwich. (2) Electrically conducting silver paint, if not also showing effects like sputtered electrodes, contains solvents and hence cannot be used on the polymers. (3) Geometrically defined metal plates under pressure can damage the thin film or do not result in a defined contact area due to air gaps between the electrode and the film. (4) One may propose to stack two polymer-coated glass plates with the films facing each other. Then the

c_{chr} [mol%]	c_{chr} [wt%]	T_{G} [°C]	T_{pol} [°C]	r_{13} [pm/V]
20	54	101	106	13.5
30	67	104	114	14.3
40	76	120	122	23.3
60	88	100	110	42.5
100	100	94	102	40.3
100	100	120	110	16.7
100	100	120	116	24.4
100	100	120	118	33.4
100	100	120	128	18.8
100	100	120	135	12.4

Table 4.1: Chromophore contents c_{chr}, glass transition temperatures T_{G}, poling temperatures T_{pol}, and POCKELS coefficients r_{13} of the materials used.

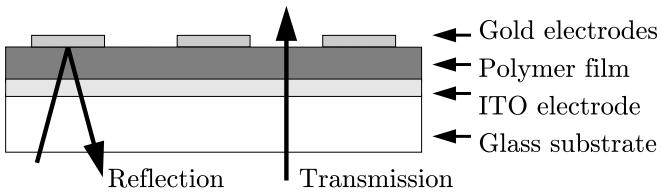

Figure 4.2: Sample geometry.

two ITO electrodes can be used to measure the conductivity. However, the processing requires to heat up the sandwich under pressure in order to fuse the two polymer films, but this would cause either a decay of any orientation previously induced or a crystallization.

For the other measurements (absorption and electro-optic), the final step of the sample preparation is the deposition of finger gold electrodes by sputtering. This is done by using an aluminum mask leaving some areas transparent for absorption measurements in transmission, while the other areas can be used in the reflection interferometer (see Fig. 4.2).

4.2 Electro-optic measurements

In order to measure the electro-optic coefficients, the samples are investigated at room temperature in a free-beam MACH-ZEHNDER interferometer first proposed by NORWOOD *et al.* [87]. This technique allows to determine the components of the POCKELS tensor independently. The coefficients are obtained by measuring phase changes due to electric-field-induced refractive index changes and calculating the electric suscepti-

bility. The actual experimental setup, measurement procedure, and calculations are described in greater detail in Ref. [88].

4.3 Refractive index measurements

For later analysis, the dispersion of the refractive index of the material is needed. Therefore, two complementary measurements are performed. For the first one, a prism coupler (Metricon) is used for waveguide spectroscopy [89]. The values are measured in TE mode (polarization in the film plane) and determined by the transmitted modes in the polymer film. The values for the TM mode are around 0.05 smaller due to a slightly anisotropic chromophore orientation caused by the spin coating process, while each corona poling procedure induces, again, minor changes. However, because of possible scratches from the prism coupler and resulting short cuts, the measurements cannot be performed for each sample after the spin coating and before the sputtering. Therefore, an nonpoled sample is chosen to be used as a reference.

In order to obtain the entire spectrum of the index values from 335 to 2240 nm, the Kramers-Kronig relation is used. For this purpose, the absorption spectrum of a dilute solution of the polymer contained in a cuvette is measured. A Varian Cary 500 spectrometer is employed.

4.4 Dichroism measurements

For determining the second order parameter the method of linear dichroism is applied [90]. The spectrometer used for investigation is, again, the Varian Cary 500. The absorption of the sample films is measured in transmission and with a beam incidence angle of $\alpha = \pi/4$ with light polarized parallelly and perpendicularly with respect to the incident plane over a wavelength region from 300 to 800 nm. This range is chosen, because there are significant absorption peaks of the rod-like chromophore side-chains, such as those that induce the photoisomerization. An ITO-coated glass plate is placed in the reference arm of the spectrometer to correct the absorption of the substrate. Prior to these measurements, the spectra of the reflectivities of the air-glass, the air-ITO and the air-polymer interfaces are measured in a modification of the same spectrometer for measurements in reflection mode. They are used to correct the recorded absorption spectra of the polymer films.

4.5 X-ray scattering

In order to confirm the experimentally obtained information about orientation with an independent source, X-ray scattering measurements have been done. The details are presented here, because the experimental results have been analyzed, interpreted and used for comparison in this thesis.

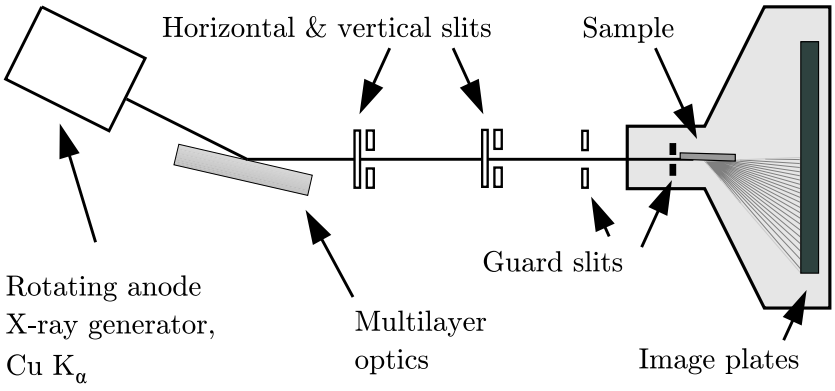

Figure 4.3: Grazing incidence wide-angle X-ray scattering setup.

Grazing-incidence wide-angle X-ray scattering (GIWAXS, Fig. 4.3) is measured. Copper $K_{\alpha,\beta}$ radiation is generated by a rotating anode operating at 10 kW and is then focused, collimated, and filtered (only Cu K_α is selected) by a multilayer X-ray mirror. Scattering from the sample substrate is suppressed, except from the topmost layers, by setting the sample surface to a very small angle with respect to the X-ray beam [91]. In this manner scattering measurements of nanometer thin films are feasible. The scattered signal was recorded on photo-stimulable image plates and later scanned. The three samples used in this experiment are made of the polymer with 100 % chromophore concentration and a glass transition temperature of 94 °C. The films are poled at 84 °C, 102 °C (the optimal temperature with respect to highest Pockels coefficients), and 124 °C.

4.6 Dielectric spectroscopy

The dielectric experiments [49] are performed using a high-resolution broadband dielectric spectrometer (Novocontrol, Alpha) over the frequency range 10^{-2} to 10^7 Hz. The sample is positioned into the sample holder (Fig. 4.4) and contacted via the ITO coating and the adhesive conductive pad. The spectra are measured at temperatures of 0, 20, 40, 60, 80, 90, and 100 °C and for some samples also at 110, 120, and 130 °C. Then the measurement is repeated at 40, 20, and 0 °C. It is interesting to observe the relaxation of the structure induced by poling during the sequence when the samples are heated up. However, there is no such kind of information to be gathered when the sample is cooled down again. Therefore, measurements are performed only at three lower temperatures in order to be able to extract the activation energy after the structural relaxation. The temperature of the samples is controlled using a cryostat with an accuracy of ± 0.1 K. Between each measurement, 15 minutes pass to allow temperature equilibration.

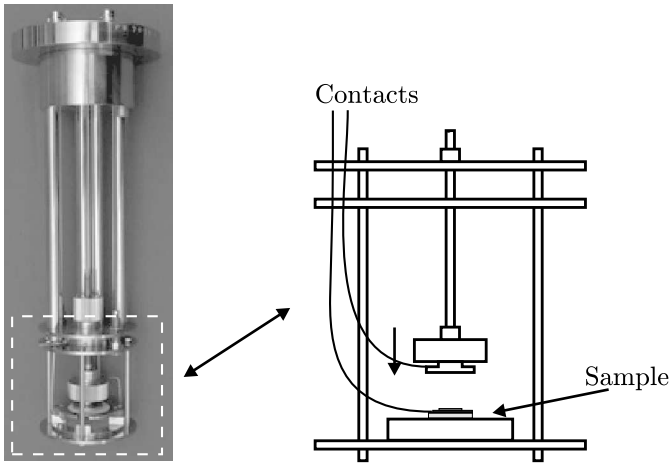

Figure 4.4: Sample holder of the dielectric spectrometer (left: photography; right: schematic depiction) to be positioned in an accurately temperature-controlled cryostat.

4.7 Ellipsometry

The experimental setup for measuring the time dependence of the birefringence is a single wavelength transmission ellipsometer [92], a modified version of the commonly employed measurement in reflection [93] proposed by Teng and Man [94]. The setup is schematically displayed in Fig. 4.5. A $\pi/4$ tilted sample (with respect to the laser beam) transmits a $\pi/4$ linearly polarized He-Ne laser beam (5 mW, λ=632.8 nm) (with respect to the incident plane of the sample). Using a quarter wave plate, a Wollaston prism, and two photodetectors, the change in refractive index of the polymer in the film plane and in the direction $\pi/4$ in between the film plane and the film normal is measured. Temperature regulation is enabled by mounting the sample on top of a Peltier element. In order to ensure an initial random orientation of the chromophores the sample is heated up to 10 K above glass transition temperature for a few minutes without poling before each measurement. Chopper triggered Lock-in detection is used to reduce the noise level.

4.8 Glass transition temperature

For the plasticized materials (containing ECZ), the glass transition could not be measured by the commonly used differential scanning calorimetry (DSC), because the phase transition is so smooth that a specific transition temperature cannot be explicitly determined. A second possibility to define the glass transition temperature, as mentioned in section 2.4, is to spot where the structural relaxation time is of the order of 100 s [95]. Therefore, dielectric measurements are performed with the dielectric spectrometer at 25 temperatures over a range, in which the glass transition temperature is expected to

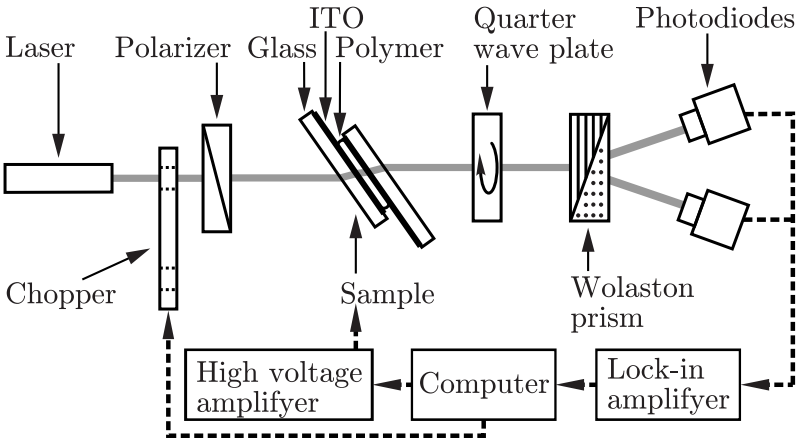

Figure 4.5: Schematic ellipsometric setup.

be found.

Chapter 5

Results and data analysis

5.1 Dipole-dipole interaction

5.1.1 Refractive index measurements

The refractive indices measured by using the prism coupler in TE mode are determined to be 1.88 at a wavelength of 685 nm, 1.74 at 1300 nm, and 1.72 at 1550 nm. In order to obtain the entire spectrum, the absorption coefficient of a solution of the material is measured. With the optical path length and the concentration of the solution, the absorption coefficient of the bulk material can be inferred. Then the KRAMERS-KRONIG relation is applied. A constant offset value has to be added to the spectrum to match the three values obtained with the prism coupler, because the integration is performed over the limited measured region of wavelengths and not over the complete electromagnetic spectrum, as required for an exact calculation. The result is shown in Fig. 5.1.

5.1.2 Density-functional calculations

Graphs *i* and *ii* of Fig. 5.2 show the absorption spectra obtained using density-functional calculations (see section 3.1). The calculations only yield peak positions and oscillator strengths (cross sections). For the illustrations, a LORENTZIAN line broadening with a uniform FWHM (full-width-at-half-maximum) of 0.4 eV has been used. The oscillator strengths associated with the excitation energies are computed from the associated transition dipole moment vectors. These vectors are dominated by the z-component, which coincides with the principal molecular axis of the chromophores. The computed absorption cross sections therefore correspond to experimental ones measured with polarized light, the electric field vector of which is parallel to the principal molecular axis. According to the present calculations, the major absorption peak of a single *trans*,*trans* chromophore has a position around 450 nm. Photochemical *trans*/*cis* isomerization results in a blue-shift of the major absorption lines. A *cis*,*trans* configuration with the *trans* NN group close to the CN group (Fig. 3.1*v*) results in a second

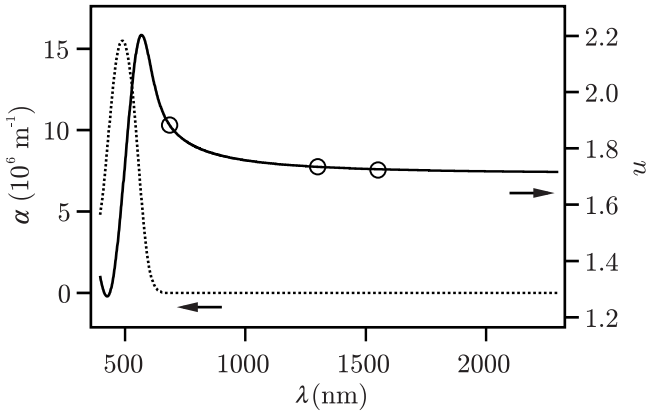

Figure 5.1: The absorption coefficient α of the polymer (dotted line) and the refractive index n (solid line) as a function of the wavelength λ. The circles indicate the values measured using the prism coupler.

major peak (now two peaks at about 410 and 360 nm, see Fig. 5.2*i*), while an isomerization of the other NN bond (Fig. 3.1*iv*) changes the shape of the curve by adding a shoulder for shorter wavelengths (peak at around 430 nm). When two *trans*,*trans* molecules are placed close to each other the change in the calculated absorption spectrum is very small for distances of 0.4 and 0.35 nm or for a skew configuration (data not shown). The two special cases, which are focussed on here, are a parallel (head-to-head, Fig. 3.1*ii*) and an anti-parallel (head-to-tail, Fig. 3.1*iii*) alignment with a distance of $d = 0.3$ nm. In the first case there is one main absorption peak at 420 nm (a shift to shorter wavelengths with respect to an isolated monomer, see Fig. 5.2*ii*) and in the second case there are two major peaks at 470 and at 420 nm.

5.1.3 Orientation distribution function

The POCKELS coefficients measured show the ratio $r_{33} : r_{13} = 3 : 1$. Assuming the orientated gas model [11], the POCKELS coefficients have been shown to follow this relation [96]. Even though higher values have been measured for this ratio [87], the approximation has proved valid for many polymers [97], especially for the ones under investigation in this thesis [88]. This leads us from the Eqs. (2.12) and (2.13) to

$$a_1 = \frac{1}{fN\beta_{zzz}} 5r_{13} \quad \text{and} \tag{5.1}$$

$$a_3 = 0. \tag{5.2}$$

The first order parameters, calculated with these Eqs. are displayed in Fig. 5.3 as functions of the chromophore concentration (graph *i*, open circles) and as a function of the poling temperature (graph *ii*, open circles). The first order parameter is lower in materials with low chromophore concentrations, increases until about 90 wt%, and

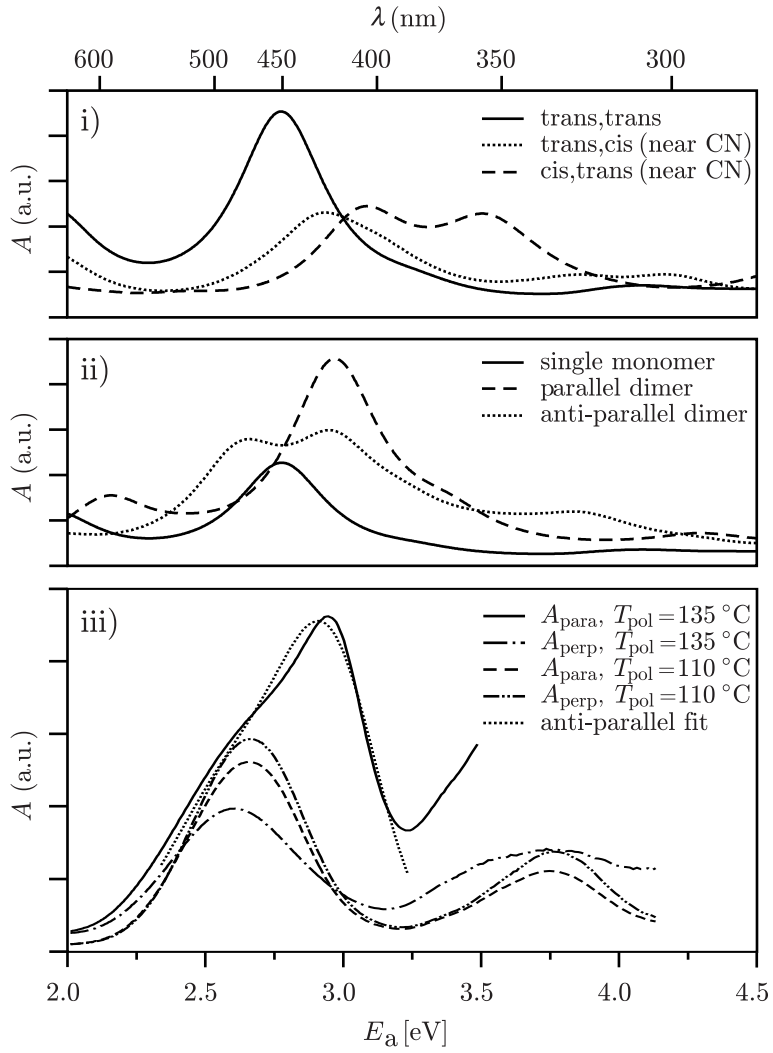

Figure 5.2: Spectra of absorption A as a function of the wavelength λ and as a function of the photon energy E_a, all with same scaling; **graph *i*:** of a *trans,trans* chromophore (solid curve; see Fig. 3.1*i*), of a *trans,cis* chromophore (dotted curve; see Fig. 3.1*v*), and of a *cis,trans* chromophore (dashed curve; see Fig. 3.1*iv*); **graph *ii*:** again, of an isolated single *trans,trans* chromophore (solid, same as in graph *i*), of a dimer in parallel (head-to-head) orientation (dashed, see Fig. 3.1*ii*), and of a dimer in anti-parallel (head-to-tail) orientation (dotted, see Fig. 3.1*iii*); **graph *iii*:** of the material with 100 % chromophore concentration poled at 135 °C measured with parallelly (solid) and perpendicularly (dash-dotted) polarized light and of the one poled at 110 °C measured with parallelly (dash-dot-dotted) and perpendicularly (dashed) polarized light. The dotted line represents a curve fit with the calculation results of the anti-parallel dimer.

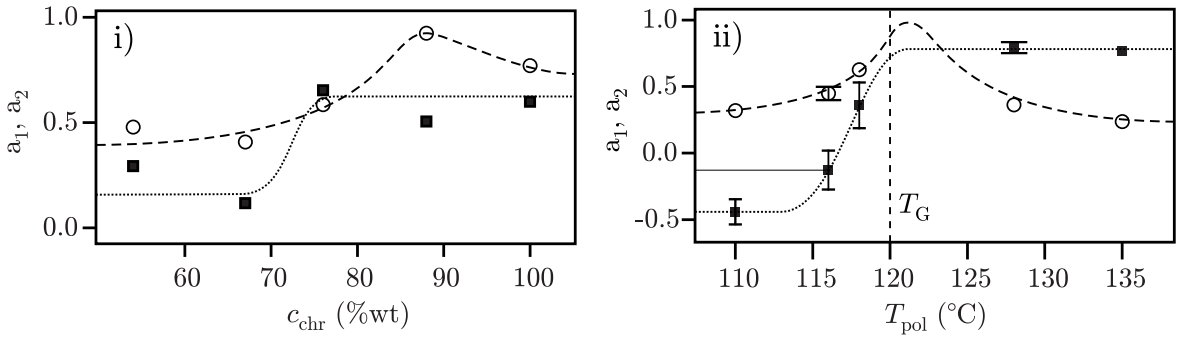

Figure 5.3: The first (open circles) and second (filled squares) order parameter a_1 and a_2 as functions of the chromophore concentration c_{chr} with each optimal poling temperature (graph *i*) and as functions of the previous poling temperature T_{pol} (graph ii). T_G marks the glass transition temperature. The dotted and dashes lines are guides to the eye representing intuitive behaviors.

then falls off again for 100 %. For the material with 100 % chromophore content corona poled at different temperatures the first order parameter rises as the poling temperature increases. However, above the glass transition temperature, the coefficients decrease again.

Graph *iii* in Fig. 5.2 shows examples of the absorption spectra of two polymer films, one previously poled well below and the other one well above the glass transition temperature, measured with light of parallel and perpendicular polarization. All spectra show strong absorption for wavelengths between 380 and 600 nm. The sample poled at 135 °C (solid and dash-dotted curve) shows broader peaks than the one poled at 110 °C (dashed and dash-dot-dotted curve). With light polarized parallelly to the plane of incidence, apart from the peak noticed in all other curves at around 470 nm, a second large peak at shorter wavelengths (around 420 nm) appears in the spectrum of the sample poled at high temperature leaving the first one like a shoulder of the curve. One should note that the dichroic ratios of the two samples, calculated by dividing the absorption of parallelly polarized light by the absorption of perpendicularly polarized one, are qualitatively inverse to each other.

In the following, the shape of the measured spectra is described. The density-functional calculations performed provide excitation energies and corresponding oscillator strengths. While the former trivially give information about peak positions, the latter ones correspond to the integral over a peak in an absorption spectrum. Information about the line width of a peak is not given, since line shapes depend highly on the molecular environment and other influences. Of course, peaks in the measured spectra also occur for wavelengths shorter than 380 nm, but they are not required for evaluation of the orientation of the dipolar side-chains, since the absorption peaks under investigation are known to correspond to the rod-like π-orbitals of the chromophores. A curve fit is performed to the absorption spectrum measured with parallelly polarized

light on a film poled at 135 °C (solid curve in Fig. 5.2*iii*), using the calculated line spectrum for an anti-parallel dimer (represented as the dotted curve in Fig. 5.2*ii* with an FWHM of 0.4 eV). Only the two most pronounced calculated lines are used (actually, two clusters of two and three lines, respectively; one at around 2.62 eV and the other one at around 2.96 eV). While the two peak positions and the ratio of their integrals is kept constant, only the two line widths (FWHM), and therefore the maxima, are left to be free curve fit parameters. The result is plotted as the dotted curve in graph *iii* in Fig. 5.2.

The analysis of the absorption data and the calculations of the second order parameters is performed as follows. The dichroic ratio has to be calculated for wavelengths, to which mainly the rod-like chromophores respond. However, for the different samples and the two polarizations, the peaks are at distinct positions with varying amplitudes. Therefore, this cannot be done at a single wavelength. The absorption peaks are integrated over windows consisting of the combined full width range of the individual spectra measured with parallelly and perpendicularly polarized light at the empirically chosen value of $1/e$ of the peak maximum. Peaks at wavelengths shorter than 400 nm are neglected.

Then, the calculation of the order para Eqs. (2.14) and (2.15) is done with those values. The results are also shown in Fig. 5.3. At low chromophore concentrations and at low temperatures, the second order parameters are low, yielding even negative values for low temperatures. As the concentration rises to higher than 70 wt%, higher values for a_2 are obtained. The behavior is even stronger pronounced as the poling temperature is increased in the high concentration material having a significant rise from the almost smallest possible to the largest possible values of a_2 within only a few degrees.

Subsequently, the orientation distribution functions (ODFs) are calculated using Eq. (2.4) up to the third order. They are displayed in Fig. 5.4. In all samples with different chromophore concentrations poled at the optimal temperature with respect to the highest Pockels coefficient (graph *i*) more chromophores point into the direction of the externally applied electric field ($\theta = 0$) than opposite to it ($\theta = \pi$). However, head-to-tail orientation (neighboring chromophores pointing into the opposite directions) is clearly notable. Even more interesting is the set of curves in graph *ii*. At the lowest poling temperatures 110 °C and 116 °C, a peak or a shoulder, respectively, appears at $\theta = \pi/2$. At the highest poling temperatures, 128 °C and 135 °C, almost as many chromophores point in the direction of the external electric field as against it.

The error bars displayed in Fig. 5.3 represent statistical errors. For the first order parameters they are all of the order of 10 %. For the second order parameter they depend highly on the magnitude, ranging around 5 % for the highest values, but exceeding unity for the small ones (such as for the value at 116 °C poling temperature, see Fig. 5.3). This is very understandable and due to the fact that the target of the dichroism measurements is to record a very small difference in absorption within a wavelength range, where the material is by many orders of magnitude stronger absorbing than in other wavelength regions. Another reason for the high error values is

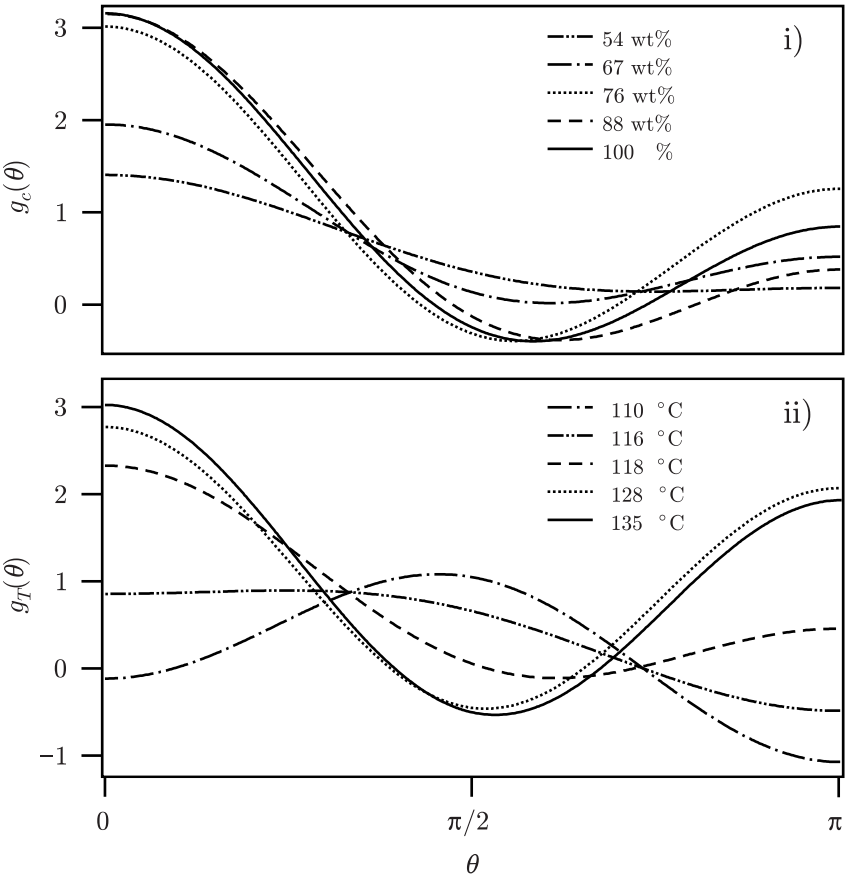

Figure 5.4: Chromophore orientation distributions as functions of the polar angle θ; **graph *i*:** for polymers with different chromophore concentrations, previously corona poled at each one's individual optimal poling temperature ($g_{\mathrm{c}}(\theta)$); **graph *ii*:** for a polymer with 100 % chromophore concentration previously corona poled at different poling temperatures ($g_{\mathrm{T}}(\theta)$).

the specific mathematical kind of interrelation between the experimentally measured properties and the calculated parameters. In special cases, it leads from rather small deviations of the absorption to large ones of the second order parameter. In order to reduce the statistical error for the crucial samples, up to 20 spectra with integration times of several seconds per recorded wavelength are measured and averaged. At the same time, the systematic errors of properties, such as the chromophore densities, are very difficult to estimate. The negative values of the orientation distributions, which are physically not meaningful, might be attributed to these systematic errors (see Fig. 5.4). However, the errors give only an offset to all second order parameters and leave the values still sufficiently accurate to be able to make qualitative comparisons of the different samples.

5.1.4 X-ray scattering

In all samples, diffuse scattering from the glass substrate is observed, as well as powder rings from cubic ITO ($d_{211} = 0.413$ nm, $d_{222} = 0.292$ nm, $d_{400} = 0.253$ nm). Figure 5.5 shows diffraction patterns of polymer samples corona poled at three different temperatures. Besides the recorded scattering signals, ordering is schematically proposed in the right column of the figure. Graph *i* shows the scattering from the sample poled at 84 °C, well below glass transition temperature. A phase with in-plane order is observed with a periodicity of 1.35 nm. The scattering signal is not a single peak, but rather broad and very weak, however still detectable. The material is largely disordered. The diffracting structures are small and distributed over a wide angle. Graph *ii* shows the scattered X-ray pattern of a sample, which has been poled at 102 °C (the optimal poling temperature). A phase with out-of-plane order is observed. Again, the diffracted signal does not consist of single peaks, but broad quarter circles implying a distribution of diffracting structures around a perpendicular position with respect to the film normal. However, the signal is stronger. The positions of the signals correspond to the first and the second order of diffraction from these structures with a periodicity of 2.7 nm. The diffracting structures are bigger and, again, distributed over a wide angle. Finally, shown in graph *iii*, the sample poled at 124 °C yields the sharpest peaks, both azimuthal and radial, revealing the highest order, again, out-of-plane with a structure periodicity of 2.7 nm. The diffracting structures are bigger (smaller radial broadness) and more oriented (smaller azimuthal broadness). All graphs are shown with the same scaling. The gray scale has been adjusted suitably for each graph in order to be able to identify the diffraction maxima.

5.2 Conductivity

In order to estimate the influence of the adhesive conductive pad, the measurement sequence is performed on a pad attached to an ITO glass plate without a polymer film. The results show very high conductivities. Thus, in the real measurements, indeed the polymer limits the conductivity and is studied.

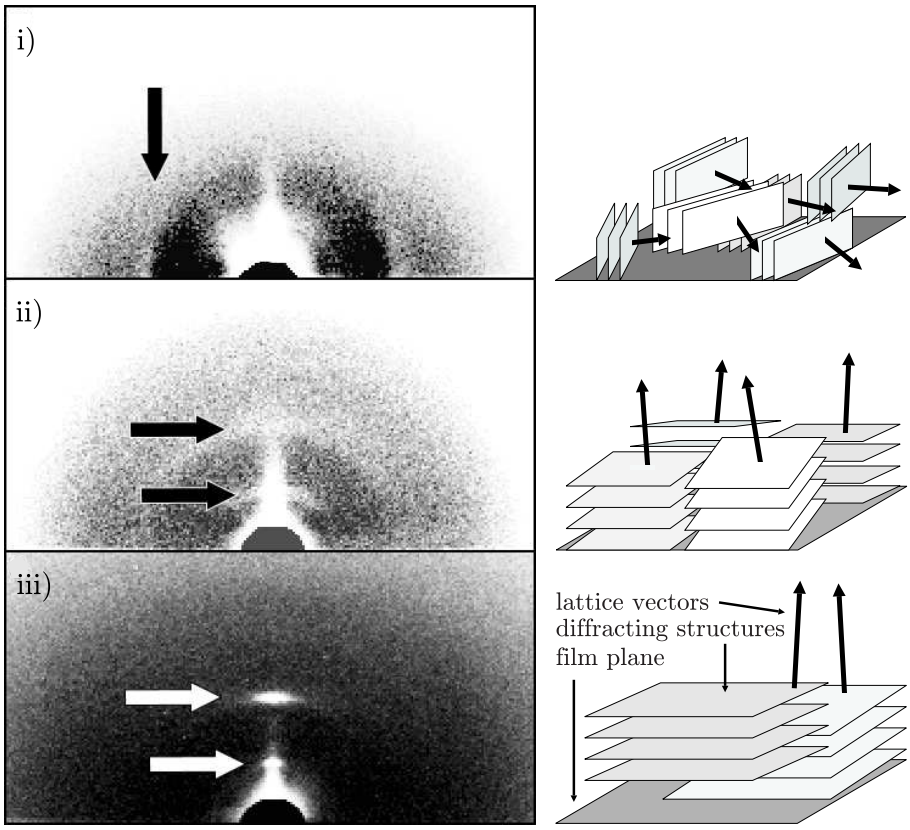

Figure 5.5: X-ray scattering images (left) of polymer films with 100 % chromophore content and a glass transition temperature of 94 °C poled at 84 °C (**graph *i***), 102 °C (**graph *ii***), and 124 °C (**graph *iii***). The right column schematically represents according diffracting structures with respect to the horizontal film pane: very small domains with very few diffracting planes and a large angular distribution with in-plane order (***i***), small domains with few diffracting planes and still a large angular distribution with out-of-plane order (***ii***), and larger domains with more diffracting planes and a small angular distribution, again, with out-of-plane order (***iii***).

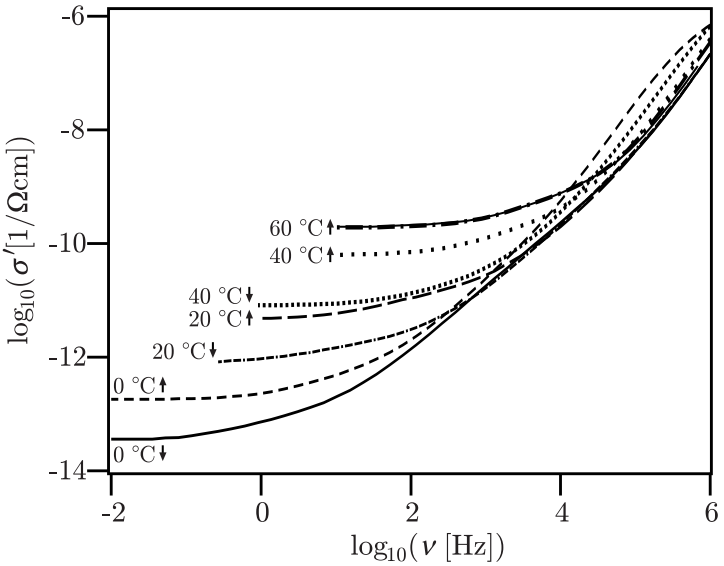

Figure 5.6: Real part of the conductivity of a polymer film poled at 104 °C and measured at 0, 20, 40, 60 (before being heated up to 100 °C, arrow up), and 40, 20, and 0 °C (after cooling down, arrow down) as a function of the frequency on a double-logarithmic scale. The thin solid line is a curve fit of Eq. 2.24 to the experimental data for 60 °C (thick dash-dotted line) with typical fit quality.

The choice of solvent has a noticeable effect on the measured conductivities. Films cast from a tetrahydrofuran (THF) solution show low conductivities and often, the conductivity does not become a constant at low frequencies, hence no DC conductivity can be determined. Films cast from cyclopentanone, however, show DC conductivity levels at least an order of magnitude higher than those of corresponding films cast from THF.

5.2.1 Heating up to the glass transition

From the dielectric measurements, the complex conductivity is extracted. Figure 5.6 shows a typical example of the real part of the conductivity as a function of the frequency when the sample is not heated much above the glass transition temperature. The different curves represent measurements at various temperatures with a sample previously corona poled at a temperature of 104 °C. As expected, the curves show an increase for higher frequencies and approach a constant DC value as the frequency decreases. While the curves largely overlap in the high frequency regime, the levels at low frequencies order by the measurement temperature. A higher temperature generally yields a higher conductivity. After having been heated up to the glass transition temperature T_G and subsequently cooled down again, the levels are significantly lower than those measured at the same temperature before heated up. However, not for all

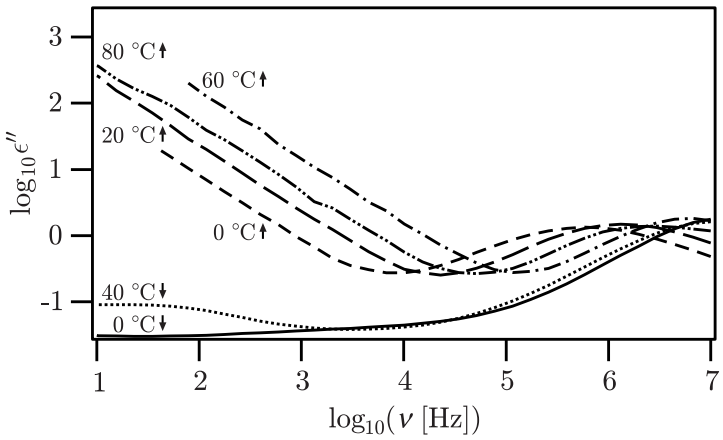

Figure 5.7: Frequency dependence of the imaginary part of the dielectric response ϵ for a sample with 100% chromophore content poled at 102 °C.

samples that are poled at different temperatures and for all measurement temperatures, an asymptotic approach towards a frequency-independent DC value of the current can be observed within the frequency region measured. In some cases the real part of the conductivity continues to decrease with the frequency.

Figure 5.7 shows the imaginary part of the dielectric permittivity, which is proportional to $\sigma/(2\pi\epsilon_0\nu)$. The same data as in Fig. 5.6 is displayed, but it shows new important features. Besides an increase towards lower frequencies with a slope of -1, which can be attributed to a frequency-independent conductivity behavior, dielectric relaxation loss peaks are observed more clearly in this plot. In this case, the term *relaxation* corresponds to resonances in the frequency space and is not to be confused with a relaxation of the material from a poled state into an equilibrium, which only occurs in the glass transition region. After cooling the sample down again, this conductivity increase is diminished, while the loss peak moves to higher frequencies, being less temperature dependent. Except from the curve representing the measurement at 40 °C after cooling down, where an additional shoulder can be observed, only one peak is visible.

5.2.2 Heating above the glass transition

If the sample is heated up to higher temperatures, the conductivity shows the behavior displayed in Fig. 5.8. Above a certain temperature, the conductivity rises by several orders of magnitude for frequencies around 100 Hz. After cooling down, the conductivity does do not fall any more to the values lower than those before heating. Moreover, the levels at the lower temperatures after heating are substantially closer together (dotted and solid curve in Fig. 5.8).

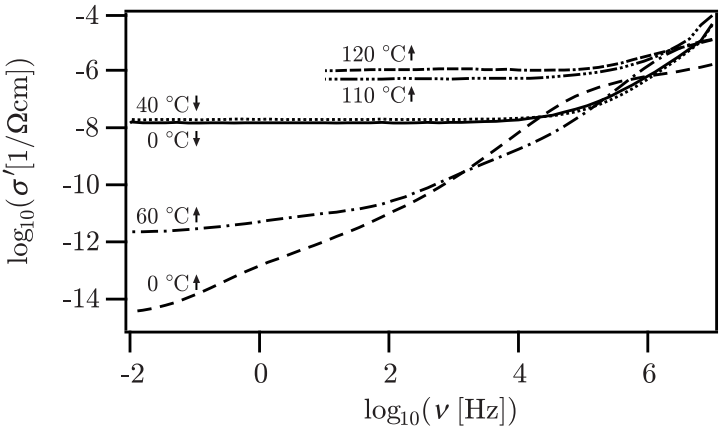

Figure 5.8: Real part of the conductivity of a film poled at 106 °C, measured at 0, 60, 110, and 120 °C (arrow up), after cooling down again at 40 and 0 °C (arrow down).

5.2.3 DC conductivity

The differences in conductivity properties between samples produced with THF and cyclopentanone, respectively, suggest that even after many hours of drying the film in a vacuum oven at 80 °C, ionic impurities from residuals of at least one of the solvent species must be still present in the polymer after the solvent has been evaporated. While this fact is not relevant for most applications and might pass unrecognized, for conductivity measurements in insulating polymers this can make a difference.

As already mentioned, not for all temperatures and for all samples, an asymptotically approached DC value exists in the conductivity spectra (such as not for Fig. 5.8, 0 °C↑). However, if the conductivity does level off, the DC value is extracted by fitting Eq. 2.24 to the experimental data, such as those shown in Figs. 5.6 and 5.8. The results are displayed in Figure 5.9 and show a typical behavior of the natural logarithm of this DC conductivity σ'_{DC} as a function of the inverse measurement temperature. At low temperatures the curve follows nearly linear, Arrhenius or Vogel-Fulcher-Tammann (VFT) behavior. After having been heated up to above the glass transition temperature and subsequently cooled down again, the samples do show different values of the direct current conductivity. This leads to the conclusion that the polymer films do not relax into identical isotropically disordered states. Thus, the samples cannot be calibrated with respect to their final low-temperature conductivities. However, the slopes of the two curves before and after heating up to 100 °C are similar. As the temperature increases, the behavior changes dramatically in a non-linear way to lower values such that the values for the highest measured temperatures (90 and 100 °C) appear on the linear fit to the curve measured after cooling down again. This dependence is observed for all samples, although the conductivities themselves differ from film to film by up to two orders of magnitude.

It is not easy to estimate the errors, since systematic errors of the high resolution

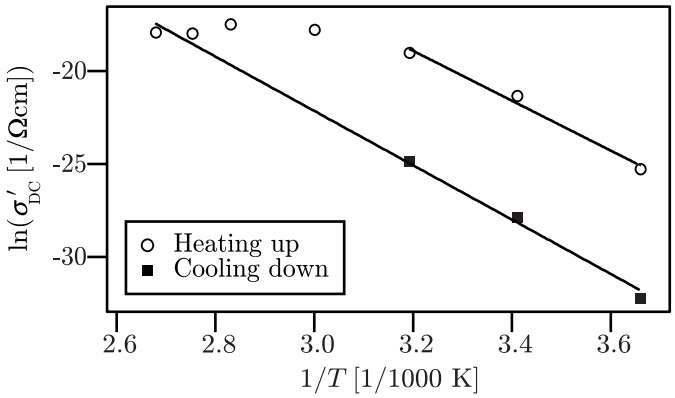

Figure 5.9: Natural logarithm of the real part of the DC conductivity σ'_{DC} obtained by fitting Eq. 2.24 to the measured frequency-dependent conductivity data (Figs. 5.6 and 5.8), here displayed as a function of the inverse temperature for a sample poled at 84 °C. Two VFT curve fits are plotted as well.

spectrometer and the data analysis are much lower than any random error induced by the film production and processing, such as the spin coating or the corona poling. Thus, it is certain that the values obtained for each sample match the real properties within a few percent. In how far the values are representative for samples of given processing can, unfortunately, only be speculated. However, experiences with measurements on many films can give us an intuitive estimation of about $10 - 15\%$ error.

Assuming the system to follow an VFT behavior within the low temperature region and fitting Eq. 2.25 to the DC conductivities, the activation energy of the conduction $E_{\mathrm{a},\sigma}$ can be extracted. Figure 5.10 displays those activation energies as a function of the poling temperature before heating up to the glass transition temperature (squares). With higher poling temperature the activation energy increases slightly.

5.2.4 Relaxation and conduction

Ionic conduction depends on structural changes in the molecular environment of the material: Side groups have to give way to moving ions. The imaginary part of the Havriliak-Negami-function (Eq. 2.22) is fitted to the peak region of the data shown in Fig. 5.7 (10^5 to 10^7 Hz). The obtained loss peak height $\Delta\epsilon''$ in the imaginary part has an averaged value of 6.4, a standard deviation of 0.27, and represents the decrease of the permittivity ϵ_s to ϵ_∞, when the frequency moves from small to infinite values and the material cannot respond to the electric AC field anymore. Of course, besides the dielectric and the electronic response, there are also vibrational and intermolecular relaxations in the microwave region, as well as atomic relaxations. However, these frequency regions cannot be covered with a dielectric spectrometer. Moreover, their influence on the dielectric permittivity can be estimated as rather small, because the measurements performed show already low values of ϵ. Thus, as the best approximation

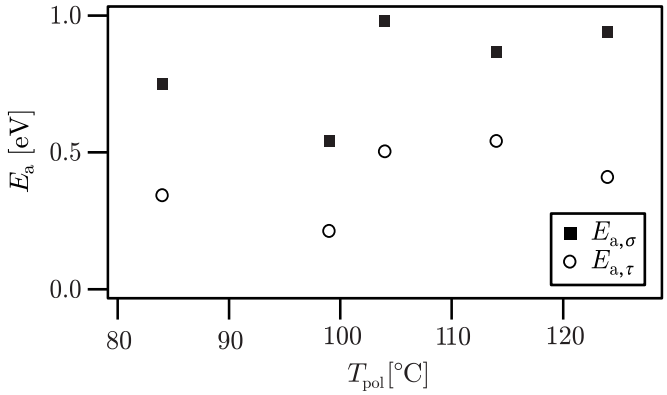

Figure 5.10: Activation energies as a function of the previous poling temperature obtained from the VFT curve fits of the DC conductivities (squares) and of the relaxation times (circles).

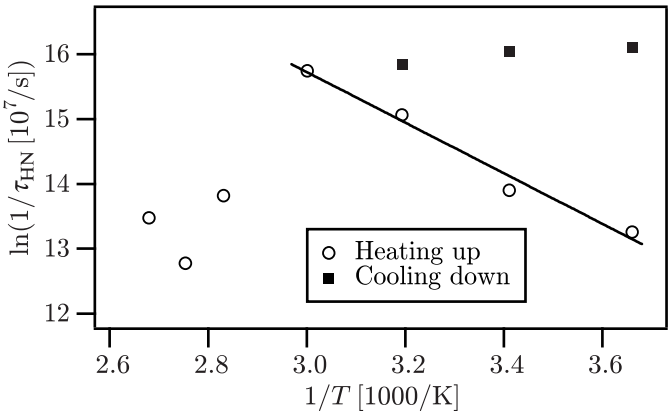

Figure 5.11: Natural logarithm of the inverse relaxation time as a function of the inverse temperature for a sample poled at 102 °C and an Arrhenius fit.

here possible, atomic relaxation and relaxation in the microwave range are neglected. The value of ϵ_∞ can be estimated from measurements of the refractive index (see section 5.1.1) to be $\epsilon_\infty = 2.9$. Using Eq. 2.21 and the values for ϵ_∞, ϵ ($\epsilon_\infty + \Delta\epsilon$), N, and T, a dipole moment of $\mu = 3.4$ D causing the loss peak in the dielectric spectrum of Fig. 5.7 ($10^5 - 10^7$ Hz) is derived.

Figure 5.11 shows the natural logarithm of the inverse relaxation times τ_{HN} versus the inverse temperature. The behavior is as expected up to 60 °C, when it drops dramatically. When cooled down again, an Arrhenius behavior cannot be noticed any more. The values are very close together. However, the relaxation peaks for those curves are close to the frequency limit of the apparatus (curve for 40 and 0 °C after cooling down in Fig. 5.7 at 10^7 Hz) and their data cannot be entirely trusted, except from the fact, that the relaxation occurs faster than in the cases when still being heated

up.

A strong dielectric relaxation observed for liquid side-chain polymers is often related to the fluctuation of dipole moments around the local director axis [98]. It is also observed for azo benzene mesogenics [99]. The relaxation observed at MHz frequencies (Fig. 5.7) can likely be assigned to the same kind of mechanism. In order to investigate whether a correlation exists between the observed behavior of conductivity and the structural relaxation, the activation energies $E_{\mathrm{a},\tau}$ and $E_{\mathrm{a},\sigma}$ of the relaxation process and the conduction, respectively, are derived and compared. Therefore, Eq. 2.26 (Arrhenius behavior) is fitted to the data in the low temperature regime of Fig. 5.11 before heating up to the glass transition. Here τ_0 is the zero temperature relaxation time. The extracted activation energies $E_{\mathrm{a},\tau}$ are also displayed in Fig. 5.10 (circles). A correlation between the two data sets can be clearly noted as the ratio between the two activation energies stays rather constant.

Within the scope of this investigation, also a series of measurements have been executed to acquire the conductivity as a function of the chromophore concentration. Unfortunately, the results have not been clearly interpretable and consistent enough for the author to decide to present them in this thesis. Of course, it can be assumed that a change of the chemical composition of the material, such as of the chromophore concentration, also modifies properties like the electric conductivity.

5.3 Glass transition temperature

For the guest-host materials, the glass transition temperature is determined using dielectric spectroscopy. A conductivity contribution and the imaginary part of two Havriliak-Negami-functions [47] (Eq. 2.22, see also Fig. 2.9) are fitted to the imaginary part of the dielectric permittivity spectra at various temperatures. The relaxation times for the material 1 (see on page 28) obtained from the curve fits are shown in Fig. 5.12, where a dashed line marks 100 s. The α-relaxation passes this value at 71.5 °C.

5.4 Polymer dynamics

In the following, the ellipsometry measurement results are presented of temporal relaxation behavior in the guest-host polymer thick films when perturbed from an unpoled equilibrium by a strong externally applied electric field. Figures 5.13*i* and *ii* show a curve displaying the normalized evolution of the birefringence of a film consisting of guest-host material 1 at a temperature of 75 °C when a voltage of 3 kV/μm is applied (solid line). The material undergoes a transition from being isotropic towards an asymptotic approach of a constant value. Figure 5.13*iii* exhibits curves for different temperatures and for the other material mixtures containing more or less plasticizer while keeping the amount of PMMA constant.

The data is analyzed in different ways: graph *i* shows a curve fit on linear time

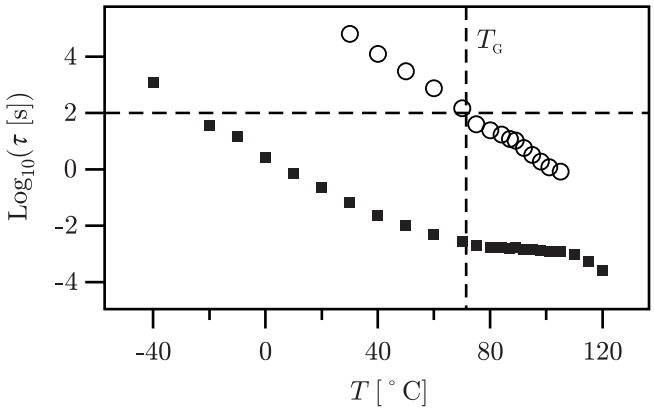

Figure 5.12: Relaxation times τ_α (circles) and τ_β (squares) of the α- and β-relaxation obtained from dielectric spectroscopy.

scale (experimental data equally spaced on linear scale) using a stretched exponential function shown in Eq. 2.27. The same curve fit appears also as the dotted line in the lower graph. The value for the characteristic relaxation time is determined to $\tau_{\mathrm{K,lin}} = 3.2$ s. Furthermore, two other curve fits are performed: both with data equally spaced on a logarithmic time scale. The first one, again, with only one KWW function (Eq. 2.27, dash-dotted line) and the other one (dashed line, almost overlapping the solid line) with a sum of two KWW terms given by

$$\phi(t) = \phi(\infty)\Big[(1 - A\ \exp(-(t/\tau_{\mathrm{K},\alpha})^{\xi_{\mathrm{K},\alpha}}) - (1-A)\ \exp(-(t/\tau_{\mathrm{K},\beta})^{\xi_{\mathrm{K},\beta}})\Big], \tag{5.3}$$

where the indices α and β represent an affiliation to the corresponding relaxation process. Here, in order to be able to make a statement about the entire relaxation, one KWW function is assigned to each process (α- and β-relaxation). One might object that using a function like this, including a higher number of free parameters, gives, of course, a better curve fit. However, the main objective is to extract the stretching parameter ξ and the characteristic relaxation time τ_{K} for each process. The values obtained are $\tau_{\mathrm{K,log}} = 0.75$ s, $\tau_{\mathrm{K},\alpha} = 18.4$ s, and $\tau_{\mathrm{K},\beta} = 0.029$ s, where the index *log* means that the according curve fit is done with data equally spaced on logarithmic time scale.

The stretching exponents ξ obtained by the curve fits are shown in Fig. 5.14. The parameter of the fits with Eq. 2.27 to data equally spaced on logarithmic time scale ($\xi_{\mathrm{K,log}}$, crosses) does not show a notable temperature dependence at all. The other two parameters are obtained using Eq. 5.3 assigning $\xi_{\mathrm{K},\alpha}$ (squares) to the α- and $\xi_{\mathrm{K},\beta}$ (circles) to the β-relaxation process.

As already observed previously in literature it a zero temperature value different from zero exists, ξ approaches a minimum value. However, comparing the three highest values for $\xi_{\mathrm{K},\beta}$ with the temperature behavior of Eq. 2.30, it appears that, furthermore,

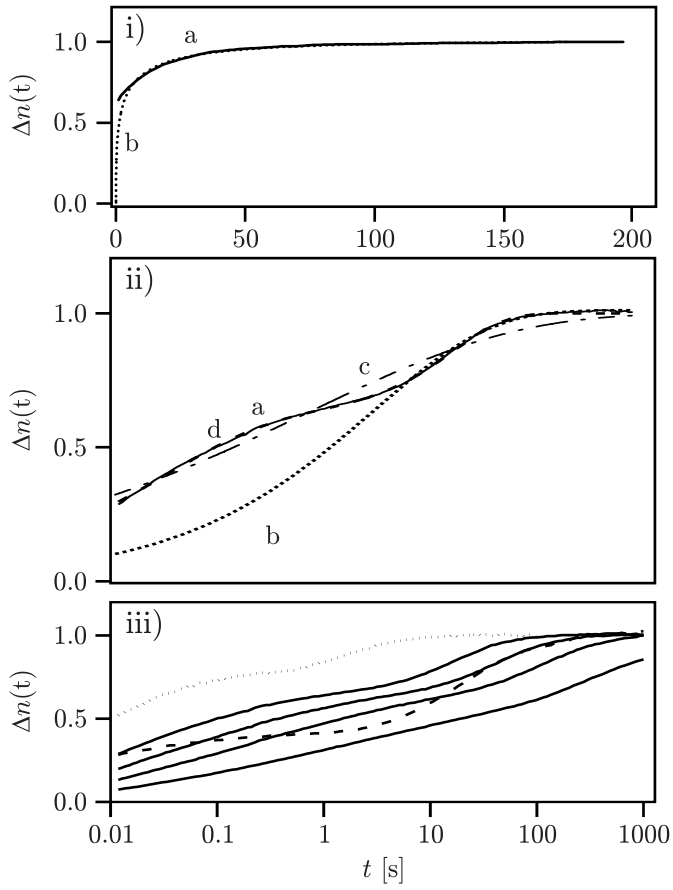

Figure 5.13: Normalized birefringence as a function of time at 75 °C. **Graph *i* and *ii*:** solid lines (a) on a linear (graph *i*) and on a logarithmic (graph *ii*) time scale. The dotted lines (b) are one curve fit with one KWW function (Eq. 2.27) to data equally spaced on linear scale displayed once in linear time scale (graph *i*) and on logarithmic time scale (graph *ii*). The dash-dotted (c) and the dashed lines (d) are curve fits to data equally spaced on logarithmic time scale with one KWW function (Eq. 2.27) and with a sum of two KWW terms (Eq. 5.3), respectively. **Graph *iii*** shows data at 60, 65, 70, and again 75 °C (solid lines from bottom up) and for a material of 80% PMMA, 5% DR1, and 15% ECZ at 85 °C (dashed line) and of 80% PMMA and 20% DR1 at 100 °C (dotted line).

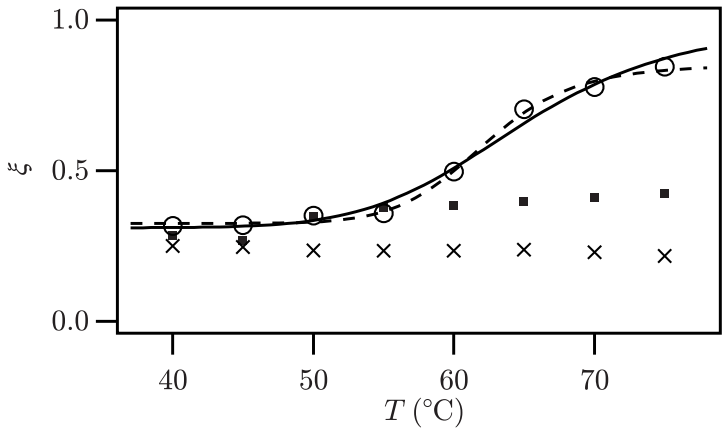

Figure 5.14: Stretching exponents $\xi_{\mathrm{K,log}}$ (Eq. 2.27, crosses), $\xi_{\mathrm{K},\alpha}$ (Eq. 5.3, squares), and $\xi_{\mathrm{K},\beta}$ (Eq. 5.3, circles) from the curve fits with one and the sum of two KWW functions. The solid line is a fit of Eq. 2.30 and the dashed line of Eq. 5.4 to the values of $\xi_{\mathrm{K},\beta}$.

for high temperatures a leveling-off occurs below the value of 1. All other curves measured in the frame of this thesis, as well as the data in Ref. [72], in which Eq. 2.30 was suggested, show exactly this feature. With values obtained from the very good curve fits using Eq. 5.3 and covering a comparatively wide temperature range, $\beta(T)$ can be suggested to be of the form

$$\xi(T) = \xi_0 + \frac{\xi_\infty - \xi_0}{2}\left[1 - \tanh\left(\frac{A}{k_\mathrm{B}}\frac{T_0 - T}{T_0 T}\right)\right], \tag{5.4}$$

where an upper limit ξ_∞ is introduced. Hereby, the averaged standard deviation drops by a factor of 4. The limiting values obtained are ξ_∞=0.85 and ξ_0=0.32.

5.5 MONTE-CARLO transport simulation

The results of the simulation are shown in Fig. 5.15 in three graphs displaying the charge carrier velocity v as a function of the orientation degree $\mathcal{E}$ (graph i), of the hopping site density ρ (graph ii), and of the driving field $D(E)$ (graph iii), while in each case the other parameters are kept constant. The constant driving field D for the data in graph i and graph ii implies that the data is identical to the normalized charge carrier mobility m.

As a function of the orientation degree, the mobility shows a lower and a higher limit. Such an increase of the conductivity has been experimentally observed in the bis-azo copolymers when undergoing a transition from a disordered to a highly ordered phase (see section 5.2.4). As the curve fit in Fig. 5.15i shows, the behavior can be

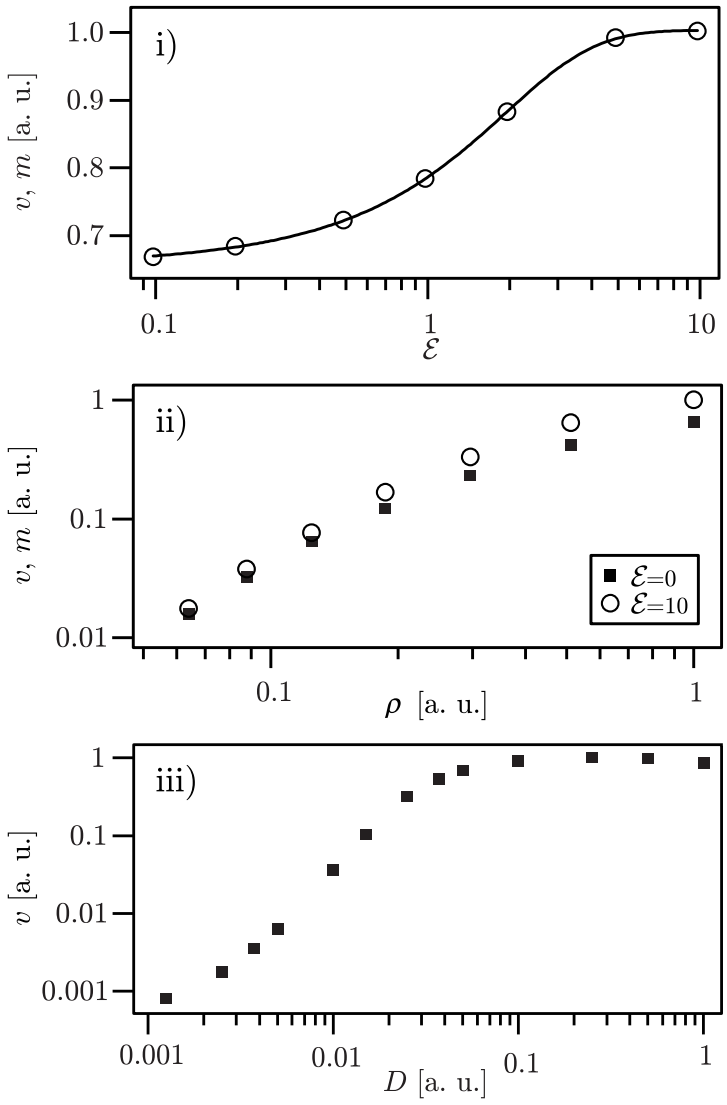

Figure 5.15: **Graph *i***: Normalized electron velocity v and normalized electron mobility m as a function of the interaction energy $\mathcal{E}$, where the curve marks the curve fit using Eq. 5.5, **graph *ii***: v and m as a function of the chromophore density ρ for two different orientation degrees, and **Graph *iii***: v as a function of the driving field $D(E)$.

surprisingly well described by a sigmoid function

$$m(\mathcal{E}) = m_0 + \frac{m_\infty - m_0}{2}\Big[1 - \tanh(a(\mathcal{E}_0 - \mathcal{E}))\Big], \tag{5.5}$$

where m_0 and m_∞ are the lower and the upper limit, respectively, $\mathcal{E}_0$ the orientation degree of the transition, and a a shape parameter. For low hopping site densities ρ, the influence of the orientation on the mobility vanishes (see left side of Fig. 5.15*ii*). Furthermore, the dependence on the density decreases as the sites get closer appearing to asymptotically approach an upper limit. Finally, the charge carrier velocity v is plotted as a function of the driving field $D(E)$ (Fig. 5.15*iii*). Over most of the lower two orders of magnitude it shows nearly a linear behavior. In the region of high fields, a saturation occurs with even a slight decrease.

Chapter 6

Discussion

6.1 Dipole-dipole interaction

By comparing the absorption spectra obtained by density-functional calculations with the measured ones (both in Fig. 5.2) the following statements can be made: The calculations support the view that the amount of molecules being in a *cis* configuration is either not existent or negligible. All molecules appear to be in a *trans*,*trans* configuration. At room temperature and at the low light intensity used by the spectrometer this is expected. The case of a *cis*,*cis* configuration is not considered for obvious reasons.

The measured absorption curves for low poling temperatures and those for high poling temperatures measured with perpendicularly polarized light match the single calculated peak of the *trans*,*trans* molecule with a deviation of about 0.1 eV. The double peak of the anti-parallel alignment is not present in the experimental spectra and the single peak of the parallel configuration shows a deviation of more than 0.3 eV. However, a quantitative agreement of the present model calculations with the experimental results should not be assumed. From these results one can deduce a weak dipole-dipole interaction after poling at low temperatures.

The spectrum for high poling temperatures measured with parallelly polarized light can be described surprisingly well with the results of the calculations for anti-parallel (head-to-tail) alignment considering that all values used are taken from gas-phase density-functional calculations (peak positions and peak integrals) and only two fit parameters (line broadenings) are left free. The broader peak positioned at lower energy (470 nm) is now only visible as a shoulder to the main peak at 420 nm (see dotted curve in Fig. 5.2*iii*). Of course, at first glance, the curve fit does not resemble the dotted curve in Fig. 5.2*ii*. However, it uses the same calculated line spectrum with the mere difference that now not all peaks have the identical FWHM of 0.4 eV. Since the spectrum of the parallel dimer (dashed curve in Fig. 5.2*ii*) does not contain a major second peak within the wavelength region in question, the necessary shoulder in the measured absorption could not be obtained and the fit (not shown) is substantially worse. Of course, one could also assume the superposition of absorption peaks caused by isolated chromophores and those in parallel orientation. However, there are three

reasons why this seems to be inappropriate: First, the ratio of the integrals of the two major peaks in *all* spectra measured at high temperatures with parallel polarization match the calculated ones of the anti-parallel orientation. Only one is plotted in this thesis. Second, the chromophores are already in a higher energy state when oriented parallelly (head-to-head) and favor relaxation towards a random orientation. The force from the dipole-dipole interaction makes an anti-parallel (head-to-tail) dipole orientation rather favorable. And third, there is no obvious reason why the absorption peak should broaden, if the majority of the chromophores goes into a head-to-head liquid-crystalline phase decreasing the overall disorder in the material. Because of all that, it can be assumed that after poling at a high temperature, the majority of the chromophores stick out of the film plane in an anti-parallel orientation, not being detected with perpendicularly polarized light, giving less absorption (dash-dotted curve in Fig. 5.2*iii*).

The results for the order parameters (Fig. 5.3) are not entirely as expected. One would think that for low chromophore concentrations the first order parameter must be at least as high as for higher concentrations (graph *i*, circles), because the dipole-dipole interaction is smaller. This is not observed and it can only be speculated about the reasons. All other results are consistent with the intuitive picture: As the poling temperature increases, and therefore the rotational mobility, at first the first order parameter increases, the chromophores can align better in the externally applied electric field. However, at even higher temperatures, the dipole-dipole interaction forces the chromophores into a head-to-tail orientation, forming a liquid crystalline phase, diminishing the inversion symmetry and therefore the first order parameter, while the second order parameter increases steadily. An increasing amount of chromophores in anti-parallel arrangement can also be seen for higher chromophore concentrations, where dipole-dipole interactions also increase the second order parameter.

Figure 5.4 shows the orientation distribution functions. This way of displaying the results clarifies the intuitive picture obtained in the previous paragraph and from Fig 5.3. After spin coating, the chromophores are largely disordered (with a broad distribution) in the film plane ($\theta = \pi/2$) (lowest temperature in graph 5.4*ii*). In fact, the ordering of side groups can be attributed to the mechanical features of the spin-coating process itself. This effect has been investigated for other polymers and various film thicknesses by, for example, comparing orientation in spin coated films with the one in LANGMUIR-BLODGETT films [100, 101]. As expected, the anisotropy vanishes when the film is heated up to the glass transition region of the material [102]. Poling at high enough temperatures increases the orientation along the field ($\theta = 0$), while still keeping opposite orientation ($\theta = \pi$) low. Increasing the rotational mobility at higher poling temperatures makes a second peak against the field appear. The strong dipole-dipole interaction leads to crystalline head-to-tail orientation. Choosing the optimal distributions for different chromophore concentrations with respect to the electro-optic response (graph 5.4*i*), there is a trade-off between obtaining the largest response by increasing the chromophore concentration and decreasing it, when the dipole-dipole interaction dominates.

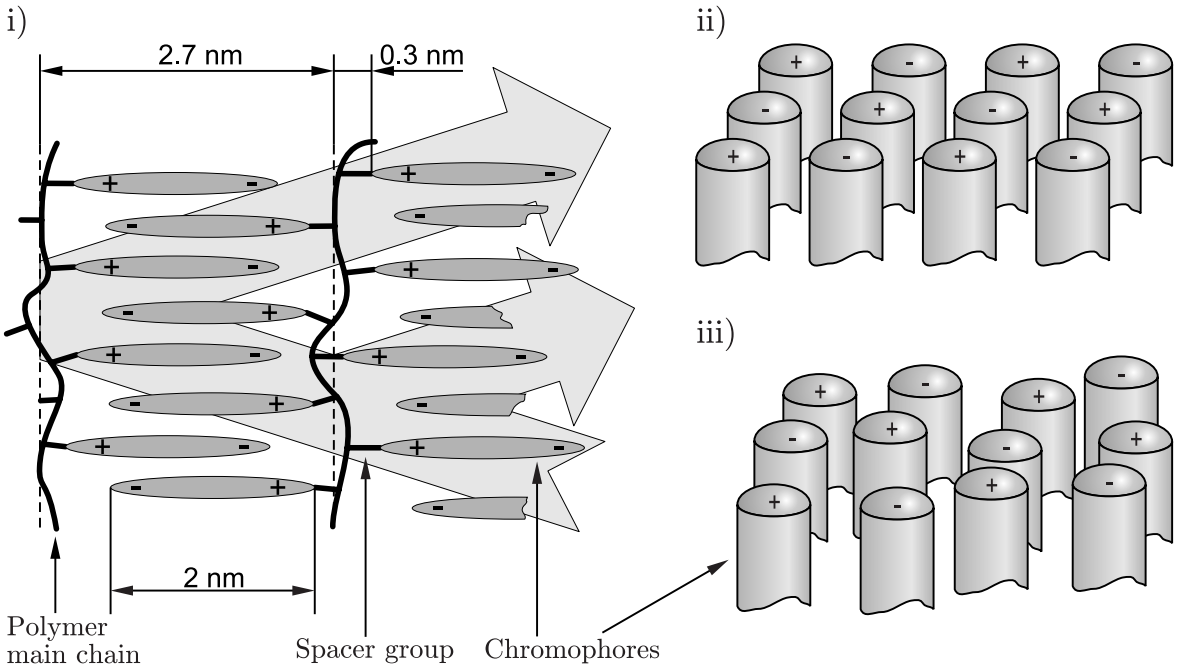

Figure 6.1: Schemes of diffracting elements. **Graph *i***: atactic head-to-tail orientation of the chromophore side groups bound by spacer groups to the polymer main chains, approx. lengths and distances. The light grey arrows in the background represent the X-ray diffraction. **Graph *ii***: periodic ordering of the chromophores in a plane. **Graph *iii***: non-periodic ordering of the chromophores.

It should be mentioned that the cooperative movements and the high chromophore density may exhibit a large birefringence in the material. Additionally, the chromophores are not cylindrically symmetric. These two properties can, in fact, result in an orientation distribution function being non-uniaxially. This biaxial orientation, where the dependence on the azimuthal angle φ cannot be neglected anymore, has been investigated in other photoaddressable bis-azo polymers [103].

Finally, the attention is drawn to the complementary X-ray scattering (Fig. 5.5). The results reveal that presumably the back bones of the polymers or just planes of oriented chromophores standing side by side and having higher electron densities than inter-plane space diffract the X-rays (see Fig. 6.1*i*). One can estimate the length of the representative monomer to be of the order of just below 2.0 nm. In combination with the derived values from the X-ray scattering, predictions about the diffracting element can only be speculations. However, with the space, which the polymer backbone occupies, and an intermolecular distance of the order of 0.3 nm, one reaches, in fact, a value of 2.7 nm for a distance of diffracting planes possibly consisting of the polymer main chains while the side chains act as spacers. In such a constellation, these side chains attached to one polymer main chain could point atactic into opposite directions and

alternate anti-parallel with every other side chain of the adjacent polymer molecule in order to form the liquid crystalline phase. The results also reveal that it cannot be a periodic ordering, as schematically displayed in Fig. 6.1*ii*, that diffracts the X-rays. The chromophores stand up in planes, but do not show sufficient periodicity for efficient diffraction. An intuitive picture can be the one shown in Fig. 6.1*iii*.

Comparing the orientation distribution functions for different poling temperatures (Fig. 5.4*ii*) with the schemes drawn from the X-ray scattering results (Fig. 5.5), both give the same information about order in the material. Order, in this sense, can be associated with the number of diffracting planes within single domains and the angular distribution of the domains' orientation (schematically displayed also in the right column of Fig. 5.5), observed as the sharpness of a peak or line in the recorded diffraction diagram. First, the highest order is obtained at the highest temperatures (with many planes parallel to the film plane). Second, at medium temperatures the order gets less pronounced (fewer diffracting planes, broader angular distribution), while the orientation of the order keeps the same (still with order out of the film plane). Third, leaving the material largely disordered, such as at the low temperatures, the order is even much less pronounced (even fewer diffracting planes) and perpendicular to the ones in the other two cases (diffracting planes perpendicular to the film plane, that is in-plane order). It is puzzling that the periodicity of the diffracting structures differs between the lowest temperature and the other two. The center in Fig. 5.5*i* is blurred, and a first diffraction order of possible structures with a periodicity of 2.7 nm cannot be detected even though it might be there. Furthermore, the diffracting distances have precisely a ratio of 2. This can indicate that, in the highly ordered material, a different phase builds up. An example for such a change is a crystallization in a centered unit-cell. Thus, the intermolecular packing distance would be still the same. However, the axis' periodicity is effectively doubled. Concluding, it can be said that the dynamics is, at least qualitatively, understood.

6.2 Conductivity

The first result found is that the choice of solvent has a noticeable effect on the measured conductivities. Films cast from a THF solution show different conductivity behavior than those cast from cyclopentanone. Several explanations may be speculated: (1) the cyclopentanone introduces ionic impurities in the polymer, which are retained in the film after all the solvent is evaporated; (2) although THF and cyclopentanone have similar overall solubility parameters, their dipole moments differ vastly, and the choice of solvent could influence the structure of the cast film; (3) either the THF or the cyclopentanone is not fully evaporated influencing the mobility of the poled film and resulting in either low stability (THF) or better charge carrier mobility (cyclopentanone) in the poled film. Certainly, the influence of the casting solvent on the electronically related properties have been observed for conjugated polymer films [104].

There is no evidence that support one explanation rather than the others and so it is chosen to report only the results for films cast from a cyclopentanone solution,

because they are more reproducible.

Secondly, it is, of course, not self evident that the electric conductivity as a function of the frequency of the applied electric field approaches a constant value for low frequencies. In the case of an insulating disordered material, the limiting factor is the buildup of a space charge field. Mobile charges, which can be ions, electrons or holes, hop (or tunnel) from one site to another and eventually they get trapped. The time a charge is confined to a hopping site is basically determined by the overlap integral of the wave functions. In the case of a random energy landscape, decreasing the frequency of an externally applied electric field allows the charge carriers to travel longer and longer until they get finally trapped. No matter how long a current has flown, the space charge field can still increase leading to no leveling-off of the frequency-dependent conductivity.

Figure 5.9, the natural logarithm of the DC conductivity as a function of the inverse temperature, does not only show, that for temperatures from 0 up to $40-60$ °C a VFT behavior can be assumed, but, furthermore, that the high temperature values appear on the same line as the conductivity values after cooling down again. In all cases when the sample is only heated up to 100 °C, these are lower than the initial ones after the corona poling. As already mentioned in section 2.3.2, generally found for DC conductivity is the empirical Vogel-Fulcher-Tammann relationship (Eq. 2.25). For real materials (metals, insulators), more different dependences on the temperature are possible besides the one suggested in this equation. However, in our case, the deviation from the linear behavior towards lower values at higher temperatures is so dramatic that it cannot be explained with a different exponent of the temperature dependence.

When the material is heated up substantially above the glass transition temperature, it does not relax into a random orientation state, but undergoes a microcrystallization process, in which the densely packed chromophores are sufficiently movable to respond with a stable head-to-tail orientation. As explained above, this order is observed by a series of experiments leading to the chromophore orientation distribution function, as well as by complementary X-ray scattering. The only two ways to go back into a disordered state is dissolving the polymer or shock freezing it from a liquid phase [27]. The induced microcrystalline order obviously entails a conductivity larger by some orders of magnitude. This means that in all our samples, even those corona poled at 124 °C, microcrystallization, if initiated, has not completed. Furthermore, if orientation is responsible for the difference of conductivities between the differently poled samples then it is to some extend able to relax when the samples are heated up to the glass transition temperature.

However, the conductivities of the polymer films after heating to the glass transition are not the same for all samples. This leads to the conclusion that after cooling down, the samples cannot be in a random disordered state like before the poling process. The only reason one can think of, that prevents the chromophores from relaxing entirely into an identical (possibly isotropic) orientation at the glass transition temperature, is a possible microcrystallization to a low extent already induced during the poling process even at low poling temperatures. It has not been investigated whether all sam-

ples reach the same microcrystalline phase when heated up sufficiently. A chemical modification during the sample preparation and the experiments can be ruled out.

Regarding the dielectric spectra (Fig. 5.7), except from the curve representing the measurement at 40 °C after cooling down, where an additional shoulder can be observed, only one peak is visible. The existence of the shoulder and the temperature behavior of these peaks suggest that they are not connected to the primary (α)-relaxation, which appears to be very weak, but rather to the secondary (β or JOHARI-GOLDMANN) relaxation caused by the dipolar bis-azo side groups.

A dipole moment causing the loss peak in the dielectric spectrum of Fig. 5.7 is calculated to be $\mu = 3.4$ D. As mentioned earlier, another numeric value for the dipole moment of 7 D has been obtained by functional density calculations on an isolated molecule. While the chromophore is bound to the polymer back bone on one end, also a partial head-to-tail orientation has been verified, which both reduce the possible orientation enhancement even further. Considering all this, a mismatch of only a factor of two is a strong indication that the loss peak in the spectra is indeed caused by a relaxation of the bis-azo side chains. Thus, the loss peak positions (Fig. 5.7), corresponding to the relaxation times τ_{HN} obtained by fitting Eq. 2.22 to the data, give information about the activation energy of the relaxation of the chromophores $E_{\mathrm{a},\tau}$. The activation energies of the relaxation $E_{\mathrm{a},\,\sigma}$ and of the conduction $E_{\mathrm{a},\,\tau}$ obtained by curve fitting, again, do show a correlation in their behavior as a function of the poling temperature (see Fig. 5.10). Thus, the dominating conduction process is limited by the movement of the side chains and can therefore assumed to be ionic.

The DC conductivity in disordered materials occurs by hopping of free charge carriers. If this kind of conduction is not ionic, in polymers it is due to hole hopping, because the energy band gap is too big for electrons to move. However, in a disordered material there are defect sites on intermediate levels, into which the electrons can be lifted and the holes can move. This happens by hopping from one molecular orbital to another. By volume the biggest amount of our material consists of bis-azo side chains, which have delocalized rod-like highest occupied and lowest unoccupied molecular orbitals of around 1.5 nm length. The probability of hopping being defined by the overlap integral will change with the orientation. A not completely occupied orbital might have a tendency to bind the hole rather at the molecule end of the electron donator. However, it will not be completely localized at one atom. No matter whether the chromophores point parallelly or anti-parallelly, orientation increases conductivity.

The behavior noted in Fig. 5.8 is typical for mixtures close to the percolation limit [105, 106], as there is a much higher leveling-off at higher temperatures. Furthermore, in our case the behavior is even more pronounced. In contrast to insulator-metal-compounds, the microcrystallites in the polymer film still grow beyond the percolation level and the conductivity jumps up without ever decreasing to original levels. Thus, conduction occurs much stronger in the liquid-crystalline phase. However, the head-to-tail orientation leaves less mobility to the ions. Conduction is dominated by hole-hopping through the π-orbitals of the oriented chromophores. For pure and randomly oriented polymers, we one can expect no leveling-off as also in PMMA. Different

film thicknesses result in different diffusion of the solvent. Comparison of the samples is therefore very critical.

6.3 Polymer dynamics

First, in order to obtain the glass transition temperature of the plasticized material, DSC measurements are found to be unsuitable. Dielectric relaxation data is used to estimate at which temperature the structural α relaxation passes with its time constant a value of 100 s. In the dielectric spectra, it can be noticed that the α-relaxation does not diverge below the glass temperature as strongly as expected and observed in other materials. This means that the material does not freeze immediately when cooled down through that region, but it undergoes a transition over a much larger region of temperatures. This smooth transition observed also by DSC measurements causes the difficulty to measure T_G by using the DSC method.

Performing curve fits to relaxation data on linear time scale is a method frequently applied in the literature [72, 107]. However, comparing the agreement between the fit using one stretched exponential function on linear time scale (dotted line in Fig. 5.13*i* and *ii*) and the experimental data (solid line in Fig. 5.13*i* and *ii*) in one graph and the other, it is clearly seen that the short time behavior is not covered. This kind of fit yields a value $\tau_{K,lin} = 3.2$ s deviating from the reasonable one of the α-relaxation, $\tau_{K,\alpha} = 18.4$ s. This can be attributed to the fact that the short time behavior (the β-relaxation) is completely ignored by describing with this function in this way. Therefore, it influences the value τ of the slow α-relaxation when obtained by curve fitting with only one term. The value $\tau_{K,log} = 0.75$ s from the curve fit of data equally spaced on a logarithmic scale falls in between the two values of $\tau_{K,\alpha}$ and $\tau_{K,\beta}$ and it does not show any representative value for either relaxation process. However, separating the analysis into the two processes in Eq. 5.3 (sum of two KWW functions) can produce reasonable results and all features (also at short times) are adequately included. The averaged standard deviation drops by two orders of magnitude as compared to the one of a fit using Eq. 2.27 (one KWW function). As mentioned earlier, modeling with two relaxation functions, one for each process, is common in the field of dielectric spectroscopy [49]. For all those reasons, it can be assumed that the values obtained for ξ to be the most representative using Eq. 5.3.

With the extreme experimental example shown, it can be argued that curve fitting using Eq. 2.27 does not lead to the temperature behavior of ξ previously suggested (Eq. 2.30). The fact that ξ as a function of temperature levels off below the value of 1 indicates that the real RTD of our physical system always remains with a non-vanishing broadness even at high temperatures. To achieve two well separated relaxation peaks is not uncommon and has been obtained using dielectric spectroscopy [50]. Analyzing experimental data in a limited region of time or on an unsuitable time scale may conceal the nature of both processes and the data analysis results in unrealistic or erroneous parameter values.

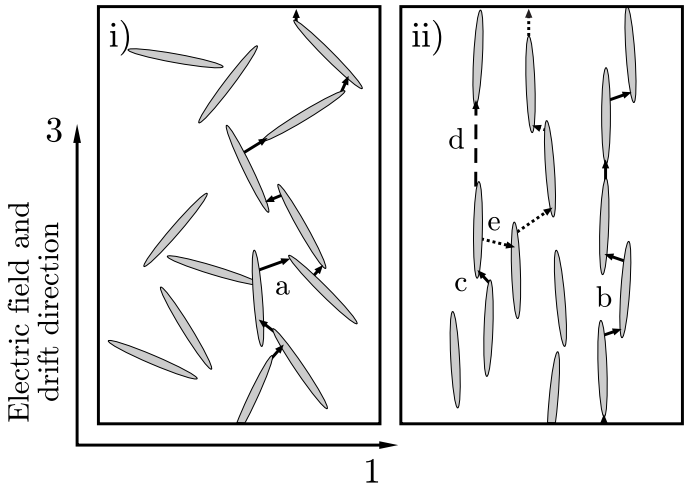

Figure 6.2: Schematic jump geometries between delocalized hopping sites. Disordered orientation and spatial distribution of chromophores (**Graph *i***) the sequence of the most probable jumps (a) consists of more and farther ones than among the highly oriented chromophores at the same center locations (**Graph *ii***), path (b). Voids ("dead ends", after jump (c)) act as traps when subsequent jumps would have to go too far (d). High fields can strengthen this influence, when "escape" paths (e) become less probable.

6.4 MONTE-CARLO transport simulation

The increase of the mobility m with the orientation $\mathcal{E}$ can be explained as follows: Figures 6.2*i* and 6.2*ii* show in 2D schematically cases of different hopping site orientations with the centers of the sites being at the same locations. As the hopping sites orient, the number and the average distance of hops can decrease (path b) with respect to the disordered case (path a). This is due to the fact the with increased orientation in the direction of the current, the distances between the ends of the rod-like hopping sites approach each other.

The influence of the orientation on the mobility decreases for low hopping site densities. This is as expected, because the hopping distance is relatively not changed substantially when the chromophores orient. The approach of an upper limit of the mobility for high densities can be explained by the fact that the number of hops increases that are necessary to cover the same distance, even though averaged hopping distances decrease, thus, making jumps more probable.

The nearly linear behavior of the velocity v as a function of the driving field $D(E)$ over two orders of magnitude and the subsequent constant values can be explained as follows: In the region of high fields, a saturation occurs with even a slight decrease of the mean velocity of the charge carriers as some of them get trapped. At densities not too high, some jumps to adjacent sites (Fig. 6.2*ii* d) are improbable due to the distance disregarding the applied field. However, if the field is substantially increased,

escape paths (e) become less probable, thus trapping the carrier in a dead end.

The nature of the dependence of D on the electric field E can be speculated about and there are two scenarios, which are presented here: (1) Considering the linear behavior of v as a function of D, the assumption of a constant real DC conductivity $\sigma'_{\mathrm{DC}} = qmN = qvN/E$ leads to the relation $D \propto E$. (2) A different dependence can be deduced when assuming the theoretically explained [108] and experimentally observed [109] universal Poole-Frenkel behavior [110], $m \propto E^{1/2}$, characteristic for conduction in disordered materials. This leads to the dependence $D \propto E^{3/2}$.

6.5 Outlook

The initial idea of investigating dipole-dipole interactions in chromophore-containing polymers has been quite fruitful, and a lot of insight has been gathered. Following this line of intentions, it would be interesting to employ the acquired knowledge one day for the development of a mathematical model describing orientation dynamics – again, as for all the other models mentioned in the introduction, by using an orientation distribution function, again plugging it into a rotation diffusion equation, and again all this using an interaction potential of the dipoles with their environment – this time, however, not only including the externally applied electric field and a local molecular field, but also the dipole-dipole interaction. For sure, a deeper understanding of dielectric and orientation relaxation will be the result, maybe bringing us also closer to an understanding of even more general phenomena, such as viscosity.

This all does not sound very practical. In connection with optical polymers and the thesis presented, the main relevant issues for applications are about the temperature stability of molecular orientation, the optimization of the orientation degree without crystallization, and its influence on material parameters, such as the conductivity, which plays a key role in many optical polymeric applications. The information given in this thesis can help to optimize those material parameters, be it geometrical or chemical ones.

Chapter 7

Summary

Within the last two decades polymers have attracted attention because of their performance and flexibility. Using these materials for optical, such as electro-optic, photorefractive or light emitting applications, orientation dynamics as well as electric conduction play key roles and influence each other. For these reasons, models have been developed to mathematically describe both.

In this thesis, experiments are made to investigate the relaxation dynamics in polymers, the orientation distribution of chromophores, as well as the influence on the various resulting conductivities. The data of the dynamics is recorded by monitoring the time dependent birefringence with the material being subject to a strong deviation from the equilibrium by an externally applied electric field. Within this frame, the ability and the limitations of the most commonly used Kohlrausch-Williams-Watts (KWW) function to describe such a type of dynamics are investigated. It is found that even if the KWW-function is suitable for representing a variety of very different relaxation processes, using such an empirical function without theoretical justification requires consideration of its applicability. By including only a single relaxation process into the description, one can obtain useful information such as the characteristic relaxation time τ_{K} or the stretching exponent ξ_{K}. However, even if the dependence (such as on temperature) follows the expectations, one has to be aware of the fact that small influences from other processes can still change the true values. Therefore, one has to focuss on only one relaxation process. This can be done by, e.g., choosing the appropriate time region. It should be clear that due to the fact that dynamics in disordered materials occur over many orders of magnitude, an analysis on a linear time scale does not make sense, since it always conceals the short time behavior. For accurately describing a more complex dynamic behavior, the KWW function is not sufficient.

Furthermore, the orientation distribution in high-chromophore-density electro-optic photoaddressable polymers is investigated. Electro-optic and linear dichroic absorption measurements, density-functional calculations, and grazing incidence wide-angle X-ray scattering are combined. For the influence of dipole-dipole interaction on the orientation distribution, the following conclusions can be consistently made: After the spin coating process, the chromophores lay in the film plane, but the material is

still largely disordered. An electric field aligns the chromophores in the direction of the poling field perpendicular to the film plane. As the mobility or the chromophore concentration are raised, a higher order is reached with a head-to-tail orientation of the chromophores, which becomes more and more pronounced for higher chromophore concentrations and poling temperatures. Finally, a liquid crystalline phase can be reached.

Moreover, in order to investigate the influence of orientation on practically relevant material properties, the electric conductivity of polymer films corona poled at various temperatures are measured below and well above the glass transition region, as well as after cooling down again. From the results, the following physical picture can be drawn: In contrast to the general expectation, even after drying the films in a vacuum oven for several hours, there are still residual ionic impurities from the solvent present. In the poled materials, still largely disordered, the conduction is dominated by ions and can be connected to the relaxation of the chromophore side groups, which have to give way in order for the ions to move through the material. This is concluded by comparing the activation energy of the structural relaxation with the one of the conduction process. When heated up to the glass transition temperature, a relaxation of the orientation occurs and the resulting conductivity decreases, while the activation energy of the conduction stays constant. When heated to higher temperatures, a liquid crystalline phase is formed, that causes two competing processes: On the one hand, the ions get more and more frozen in, because the dipolar attraction forces grow much stronger between the chromophores in the head-to-tail orientation. On the other hand, the percolation level of the much better conducting micro-crystallites is reached. The dominating charge carrier transport process is then hole hopping.

In addition, random walk charge carrier transport Monte-Carlo simulations are applied in order to be able to compare intuitive physical pictures with experimentally obtained results. This is done with randomly distributed, rod-like shaped, oriented one-dimensional hopping sites. The simulation results show that a higher orientation degree enhances the conductivity in the direction of the orientation with the existence of a lower limit in the disordered and higher limit in the ordered state. The influence of the orientation degree on the conductivity decreases with increasing hopping site density. The conductivity as a function of a driving voltage shows a leveling-off. Voids can act as traps. The increase of conductivity with orientation order is found both in the experiments as well as in the numerical simulations.

In the frame of this thesis, deep insights in the behavior of orientation distributions of chromophores in polymers, as well as their influence on electric conduction properties could be obtained. This knowledge can be useful to optimize materials and processing for applications on the one hand. On the other hand, the fundamental features found and the physical pictures drawn can help to develop mathematical models describing orientation dynamics and conduction to a more elaborate level. The potential of combining very different experiments in order to gain broader information about very specific properties could be emphasized.

Bibliography

[1] T. H. Maiman, "Stimulated Optical Radiation in Ruby", Nature **187,** 493–494 (1960).

[2] R. H. Friend *et al.*, "Electroluminescence in Conjugated Polymers", Nature **397,** 121–128 (1999).

[3] C. D. Müller, A. Falcou, N. R. Eckefuss, M. Rojahn, V. Wiederhirn, P. Rudati, H. Frohne, O. Nuyken, H. Becker, and K. Meerholz, "Multi-Color Organic Light-Emitting Displays by Solution Processing", Nature **421,** 829–833 (2003).

[4] M. Granström, K. Petritsch, A. C. Arias, A. Lux, M. R. Andersson, and R. H. Friend, "Laminated Fabrication of Polymeric Photovoltaic Diodes", Nature **395,** 257–260 (1998).

[5] P. Peumans, S. Uchida, and S. R. Forrest, "Efficent Bulk Heterojunction Photovoltaic Cells Using Small-Molecular-Weight Organic Thin Films", Nature **425,** 158 (2003).

[6] K. Meerholz, B. L. Volodin, Sandalphon, B. Kippelen, and N. Peyghambarian, "A Photorefractive Polymer with High Optical Gain and DiFfraction efficiency near 100 %", Nature **371,** 497–500 (1994).

[7] W. E. Moerner and S. M. Silence, "Polymeric Photorefractive Materials", Chem. Rev. **94,** 127–155 (1994).

[8] S. R. Marder, B. Kippelen, A. K. Y. Jen, and N. Peyghambarian, "Design and Synthesis of Chromophores and Polymers for Electro-Optic and Photorefractive Applications", Nature **388,** 845–851 (1997).

[9] M. Lee, H. Katz, C. Erben, D. Gill, P. Gopalan, J. Heber, and D. McGee, "Broadband Modulation of Light by Using an Electro-Optic Polymer", Science **298,** 1401–1403 (2002).

[10] H. Ma, A. K.-Y. Jen, and L. R. Dalton, "Polymer-Based Optical Waveguides: Materials, Processing, and Devices", Adv. Mater. **14,** 1339 (2002).

[11] J. W. Wu, "Birefringent and Electro-Optic Effects in Poled Polymer Films: Steady-State and Transient Properties", J. Opt. Soc. Am. B **8,** 142 (1991).

[12] T. G. Pedersen, K. Jespersen, P. M. Johansen, and J. Wyller, "DC and AC Electro-Optic Response of Chromophores in a Viscoelastic Polymer Matrix: Analytical Model", J. Opt. Soc. Am. B **19,** 2622–2631 (2002).

[13] K. G. Jespersen, T. G. Pedersen, and P. M. Johansen, "Electro-Optic Response of Chromophores in a Viscoelastic Polymer Matrix to a Combined DC and AC Poling Field", J. Opt. Soc. Am. B **20,** 2179–2188 (2003).

[14] R. Hagen and T. Bieringer, "Photoaddressable Polymers for Optical Data Storage", Adv. Mater. **13,** 1805–1810 (2001).

[15] R. Ou, R. A. Gerhardt, and R. J. Samuels, "Structure and Electrical Properties of Undoped Oriented Poly(Phenylene Vinylene) Films", J. Pol. Sci. B **42,** 98 (2003).

[16] D. Apitz, R. P. Bertram, N. Benter, W. Hieringer, J. W. Andreasen, M. M. Nielsen, P. M. Johansen, and K. Buse, "Investigation of Chromophore-Chromophore Interaction by Electro-Optic Measurements, Linear Dichroism, X-Ray Scattering and Density-Functional Calculations", Phys. Rev. E **72,** 036610 (2005).

[17] J. G. Grote, J. S. Zetts, R. L. Nelson, F. K. Hopkins, L. R. Dalton, C. Zhang, and W. H. Steier, "Effect of Conductivity and Dielectric Constant on the Modulation Voltage for Optoelectronic Devices Based on Nonlinear Optical Polymers", Opt. Eng. **40,** 2464–2473 (2001).

[18] N. Benter, R. P. Bertram, E. Soergel, K. Buse, D. Apitz, L. B. Jacobsen, and P. M. Johansen, "Large-Area Fabry-Pérot Modulator Based on Electro-Optic Polymers", Appl. Opt. **44,** 6235 (2005).

[19] G. R. Meredith, J. G. Vandusen, and D. J. Williams, "Optical and Non-Linear Optical Characterization of Molecularly Doped Thermotropic Liquid-Crystalline Polymers", Macromolecules **15,** 1385 (1982).

[20] M. Eich, J. H. Wendorff, H. Ringsdorf, and H. W. Schmidt, "Nonlinear Optical Self Diffraction in a Mesogenic Side-Chain Polymer", Makromol. Chem. - Macromol. Chem. Phys. **186,** 2639 (1985).

[21] A. Natansohn, P. Rochon, X. Meng, C. Barrett, T. Buffeteau, S. Bonenfant, and M. Pézolet, "Molecular Addressing? Selective Photoinduced Cooperative Motion of Polar Ester Groups in Copolymers Containing Azobenzene Groups", Macromolecules **31,** 1155 (1998).

[22] G. C. Hartley, "The Cis-Form of Azobenzene", Nature **140,** 281 (1937).

[23] K. Ichimura, "Photoalignment of Liquid-Crystal Systems", Chem. Rev. **100,** 1847–1873 (2000).

[24] B. L. Lachut, S. A. Maier, H. A. Atwater, M. J. A. de Dood, A. Polman, R. Hagen, and S. Kostromine, "Large Spectral Birefringence in Photoadressable Polymer Films", Adv. Mat. **16,** 1746 (2004).

[25] O. S. Narayanaswamy, "A Model of Structural Relaxation in Glass", J. Am. Ceram. Soc. **54,** 491 (1971).

[26] S. Chandrasekhar, *Liquid Crystals* (Cambridge Univerity Press, Cambridge, 1977).

[27] J. Stumpe, V. Shibaev, S. Kostromine, T. Fisher, L. Läsker, R. Ruhmann, and U. Claussen, "Photo-Induced Optically Anisotropic Amorphous Film Materials from Side Group Polymers", US Patent 5,543,267, (1996).

[28] F. Kajzar, I. Ledoux, and J. Zyss, "Electric-Field-Induced Optical Second-Harmonic Generation in Polydiacetylene Solutions", Phys. Rev. A **36,** 2210–2219 (1987).

[29] F. I. Mopsik and M. G. Broadhurst, "Molecular Dipole Electrets", J. Appl. Phys. **46,** 4204–4208 (1975).

[30] *Theory of Electric Polarization*, C. J. F. Böttcher, ed., (Elsevier Scientific Publishing Company, Amsterdam, 1973), Vol. 1.

[31] *Physical Properies of Crystals*, J. F. Nye, ed., (Clarendon Press, Oxford, 1985).

[32] S. Lopes, M. X. Fernandes, M. Prieto, and M. A. R. B. Castanho, "Orientational Order of the Polyene Fatty Acid Membrane Probe *Trans*-Parinaric Acid in Langmuir-Blodgett Multilayer Films", J. Phys. Chem. B **105,** 562–568 (2001).

[33] B. Nordén, G. Lindblom, and I. Jonáš, "Linear Dichroism Spectroscopy as a Tool for Studying Molecular Orientation in Model Membrane Systems", J. Phys. Chem. **81,** 2086–2093 (1977).

[34] L. B.-Å. Johansson, Å. Davidsson, G. Lindblom, and B. Nordén, "Linear Dichroism as a Tool for Studying Molecular Orientation in Membrane Systems. 2. Order Parameters of Guest Molecules from Linear Dichroism and Nuclear Magnetic Resonance", J. Phys. Chem. **82,** 2604–2609 (1978).

[35] L. B.-Å. Johansson, "Analysis and Application of Linear Dichroism on Membranes", J. Chem. Soc. Farad. Trans. II **81,** 1375–1388 (1985).

[36] C. Kittel, *Einführung in die Festkörperphysik* (Oldenbourg, München, 2002).

[37] J. Lindmayer, "Current Transients in Insulators", J. Appl. Phys. **36,** 196–201 (1965).

[38] M. Abkowitz, H. Bäßler, and M. Stolka, "Common Features in the Transport Behaviour of Diverse Glassy Solids: Exploring the Role of Disoder", Phil. Mag. B **63,** 201 (1991).

[39] K. Zimmerman, F. Ghebremichael, M. G. Kuzyk, and C. W. Dirk, "Electric-Field-Induced Polarization Current Studies in Guest-Host Polymers", J. Appl. Phys. **75,** 1267–1285 (1994).

[40] M. Ieda, "Electrical Conduction and Carrier Traps in Polymeric Materials", IEEE Trans. Electr. Insul. **19,** 162 (1984).

[41] U. Wolf, V. I. Arkhipov, and H. Bässler, "Current Injection from a Metal to a Disordered Hopping System. I. Monte Carlo Simulation", Phys. Rev. B **59,** 7507–7513 (1999).

[42] P. Debye, "Einige Resultate einer kinetischen Theorie der Isolatoren", Physik. Z. **13,** 97–100 (1912).

[43] K. Asami, "Characterization of Heterogeneous Systems by Dielectric Spectroscopy", Prog. Polym. Sci. **27,** 1617 (2002).

[44] L. Onsager, "Electrical Moments of Molecules in Liquids", J. Am. Chem. Soc. **58,** 1486 (1936).

[45] J. G. Kirkwood, "The Dielectric Polarization of Polar Liquids", J. Chem. Phys. **7,** 911 (1939).

[46] T.-W. Nee and R. Zwanzig, "Theory of Dielectric Relaxation in Polar Liquids", J. Chem. Phys **52,** 6353 (1970).

[47] S. Havriliak and S. Negami, "A Complex Plane Representation of Dielectric and Mechanical Relaxation Processes in some Polymers", Polymer **8,** 161 (1967).

[48] S. Havriliak and S. Havriliak, "Results from an Unbiased Analysis of Nearly 1000 Sets of Relaxation Data", J. Non-Cryst. Sol. **172-174,** 297 (1994).

[49] R. Bergman, F. Alvarez, A. Alegria, and J. Colmenero, "The Merging of the Dielectric Alpha- and Beta-Relaxations in Poly(Methyl Methacrylate)", J. Chem. Phys. **109,** 7546 (1998).

[50] M. Paluch, C. M. Roland, S. Pawlus, J. Ziolo, and K. L. Ngai, "Does the Arrhenius Temperature Dependence of the Johari-Goldstein Relaxation Persist above T_G?", Phys. Rev. Lett. **91,** 115701 (2003).

[51] S. R. Elliott and A. P. Owens, "The Diffusion-Controlled Model for Ionic Transport in Glasses", Phil. Mag. B **60,** 777 (1989).

[52] W. Funke and R. Hoppe, "Jump-Relaxational Model Yields Kohlrausch-Williams-Watts Behavior", Sol. Stat. Ion. **40/41,** 200 (1990).

[53] J. C. Dyre and T. B. Schrøder, "Universality of AC Conductivity in Disordered Solids", Rev. Mod. Phys. **72,** 873 (2000).

[54] E. Montroll and G. H. Weiss, "Random Walks on Lattices. II", J. Math. Phys. **6,** 167 (1965).

[55] J. Dyre, "The Random Free-Energy Barrier Model for AC Conduction in Disordered Solids", J. Appl. Phys. **64,** 2456 (1988).

[56] F. Kremer, "How to Analyse the Conduction Contribution in Dielectric Spectra?", Dielectric Newsletter 16 (2002).

[57] S. Sigaryov, "Vogel-Fulcher-Tammann Behaviour of Ionic Conductivity in $KTiOPO_4$", J. Phys. D **26,** 1326–1327 (1993).

[58] A. Alegria, E. Guerrica-Echevarria, I. Telleria, and J. Colmenero, "Non-Debye Dielectric Relaxation around the Liquid-Glass Transition of a Glass-Forming Polymer", Phys. Rev. E **47,** 14857–14865 (1993).

[59] H. Vogel, "Das Temperatur-Abhängigkeitsgesetz der Viskosität von Flüssigkeiten", Phys. Zeit. **22,** 645 (1921).

[60] G. Fulcher, "Analysis of Recent Measurements of the Viscosity of Glasses", J. Am. Cer. Soc. **8,** 339 (1925).

[61] G. Tammann and W. Hesse, "Die Abhängigkeit der Viskosität von der Temperatur bei unterkühlten Flüssigkeiten", Z. Anorg. Allg. Chem. **156,** 245 (1926).

[62] G. Williams, in *Dielectric Relaxation Spectroscopy of Polymers, Fundamentals and Applications*, J. P. Runt and J. J. Fitzgerald, eds., (Amer. Chem. Soc. Series, Washington DC, 1997), pp. 3–65.

[63] F. H. Stillinger, "A Topographic View of Supercooled Liquids and Glass Formation", Science **267,** 1935–1939 (1995).

[64] R. D. Dureiko, D. E. Schuele, and K. D. Singer, "Modeling Relaxation Processes in Poled Electro-Optic Polymer Films", J. Opt. Soc. Am. B **15,** 338–350 (1998).

[65] F. Kohlrausch, "Beiträge zur Kenntniss der elastischen Nachwirkung", Ann. Phys. - Leipzig **128,** 1–20, 207–227, 399–419 (1866).

[66] G. Williams and D. Watts, "Non-Symmetrical Dielectric Relaxation Behavior from a simple Empirical Decay Function", Trans. Faraday Soc. **66,** 80–85 (1970).

[67] J. C. Phillips, "Stretched Exponential Relaxation in Molecular and Electronic Glasses", Rep. Prog. Phys. **59,** 1133–1207 (1996).

[68] B. Sturman, E. Podivilov, and M. Gorkunov, "Origin of Stretched Exponential Relaxation for Hopping-Transport Models", Phys. Rev. Lett. **91,** 176602 (2003).

[69] P. Hetman, B. Szabat, K. Weron, and D. Wodziński, "On the Rajagopal Relaxation-Time Distribution and its Relationship to the Kohlrausch-Williams-Watts Relaxation Function", J. Non-Cryst. Solids **330,** 66–74 (2003).

[70] C. Lindsey and G. Patterson, "Detailed Comparison of the Williams -Watts and Cole-Davidson Functions", J. Chem. Phys. **73,** 3348 (1980).

[71] X. Xia and P. G. Wolynes, "Microscopic Theory of Heterogeneity and Nonexponential Relaxations in Supercooled Liquids", Phys. Rev. Lett. **86,** 5526–5529 (2001).

[72] F. Ghebremichael and M. G. Kuzyk, "Optical Second Harmonic Generation as a Probe of the Temperature Dependence of the Distribution of Sites in a Poly(Methyl Metacrylate) Polymer Doped with Disperse Red 1 Azo Dye", J. Appl. Phys. **77,** 2896–2901 (1995).

[73] D. Becke, "Density-Functional Thermochemistry. III. The Role of Exact Exchange", J. Chem. Phys. **98,** 5648 (1993).

[74] GAUSSIAN 03, M. J. Frisch *et al.*, ed., (Gaussian, Inc., Pittsburgh, Pennsylvania, 2003).

[75] T. H. Dunning, "Gaussian-Basis Sets for Use in Correlated Molecular Calculations. 1. The Atoms Born Through Neon and Hydrogen", J. Chem. Phys. **90,** 1007 (1989).

[76] E. Runge and E. K. U. Gross, "Density-Functional Theory for Time-Dependent Systems", Phys. Rev. Lett. **52,** 997 (1984).

[77] M. E. Casida and D. P. Chong, ed., *Recent Advances in DFT* (World Scientific, Singapore, 1995), pp. 155–192.

[78] G. te Velde, F. M. Bickelhaupt, E. J. Baerends, C. Fonseca-Guerra, S. J. A. van Gisbergen, J. G. Snijders, and T. Ziegler, "Pigment mass density and refractive index determination from optical measurements", J. Comp. Chem. **22,** 931 (2001).

[79] S. J. A. van Gisbergen, J. G. Snijders, and E. J. Baerends, "Implementation of time-dependent density functional response equations", Comp. Phys. Comm. **118,** 119 (1999).

[80] G. F. L. Ferreira, "Anomalous Transient-Time Dispersion in Amorphous Solids - A Comment", Phys. Rev. B **16,** 4719–4721 (1977).

[81] A. Kambili and A. B. Walker, "Transport Properties of Highly Aligned Polymer Light-Emitting Diodes", Phys. Rev. B **63,** 012201 (2001).

[82] R. Hagen, T. Bieringer, S. Kostromine, and H. Berneth, "Optical Storage Method for Rewritable Digital Data Carriers", US Patent (Bayer AG, Germany) 2,003,049,549, A1, (2001).

[83] H. Berneth, T. Bieringer, R. Hagen, and S. Kostromine, "Re-Inscribable Optical Recording Materials with Good Solubility", US Patent (Bayer AG, Germany) 2,003,113,664, A1, (2003).

[84] G. J. T. Heesink, A. G. T. Ruiter, N. F. van Hulst, and B. Bölger, "Determination of Hyperpolarizability Tensor Components by Depolarized Hyper Rayleigh Scattering", Phys. Rev. Lett. **71,** 999–1002 (1993).

[85] R. P. Bertram, N. Benter, D. Apitz, E. Soergel, and K. Buse, "Increased Thermal Stability of a Poled Electro-Optic Polymer Using High-Molar-Mass Fractions", Phys. Rev. E **70,** 041802 (2004).

[86] M. A. Mortazavi, A. Knoesen, S. T. Knowel, B. G. Higgens, and A. Dienes, "Second-Harmonic Generation and Absorption Studies of Polymer-Dye Film Oriented by Corona-Onset Poling at Elevated Temperatures", J. Opt. Soc. Am. B **6,** 733 (1989).

[87] R. A. Norwood, M. G. Kuzyk, and R. A. Keosian, "Electrooptic Tensor Ratio Determination of Side-Chain Copolymers with Electrooptic Interferometry", J. Appl. Phys. **75,** 1869 (1994).

[88] R. P. Bertram, E. Soergel, H. Blank, N. Benter, and K. Buse, "Strong Electro-Optic Effect in Electrically Poled Photoaddressable Polymers", J. Appl. Phys. **94,** 6208–6211 (2003).

[89] R. Ulrich and R. Torge, "Measurement of Thin Film Parameters with a Prism Coupler", Appl. Opt. **12,** 2901 (1973).

[90] M. A. R. B. Castanho, S. Lopez, and M. Fernandes, "Using UV-Vis. Linear Dichroism to Study the Orientation of Molecular Probes and Biomolecules in Lipidic Membranes", Spectroscopy **17,** 377–398 (2003).

[91] J. Als-Nielsen and D. McMorrow, *Refraction and Reflection from Interfaces. Elements of Modern X-ray Physics* (John Wiley and Sons, Chichester, 2000), pp. 61–106.

[92] P. M. Lundquist, M. Jurich, J. F. Wang, H. Zhou, T. J. Marks, and G. K. Wong, "Electro-optical Characterization of Poled-Polymer Films in Transmission", Appl. Phys. Lett. **69,** 901–903 (1996).

[93] F. Michelotti, G. Nicolao, F. Tesi, and M. Bertolotti, "On the Measurement of Electro-Optic Properties of Poled Side-Chain Copolymer Films with a Modified Teng-Man Technique", Chem. Phys. **245,** 311–326 (1999).

[94] C. C. Teng and H. T. Man, "Simple Reflection Technique for Measuring the Electrooptic Coefficient of Poled Polymers", Appl. Phys. Lett. **56,** 1734–1736 (1990).

[95] M. L. Lee, Y. Li, Y. P. Feng, and W. C. Carter, "Frequency-Dependent Complex Modules at the Glass Transition in $Pd_{40}Ni_{10}Cu_{30}P_{20}$ Bulk Amorphous Alloys", Phys. Rev. B **67,** 132201 (2003).

[96] K. D. Singer, M. G. Kuzyk, and J. E. Sohn, "Second-Order Nonlinear-Optical Processes in Orientationally Ordered Materials: Relationship etween Molecular and Macroscopic Properties", J. Opt. Soc. Am. B **4,** 968–976 (1987).

[97] K. D. Singer, M. G. Kuzyk, W. R. Holland, J. E. Sohn, S. J. Lalama, R. B. Comizzoli, H. E. Katz, and M. L. Schilling, "Electro-Optic Phase Modulation and Optical Second-Harmonic Generation in Corona-Poled Polymer Films", Appl. Phys. Lett. **53,** 1800 (1988).

[98] A. Schönhals, D. Wolff, and J. Springer, "Temperature Dependence of the Relaxation Rates of and Relaxation in Liquid-Crystalline Side-Group Polymethacrylates", Macromolecules **31,** 9019 (1998).

[99] R. Birenheide, M. Eich, D. A. Jungbauer, O. Herrmannschonherr, K. Stoll, and J. Wenddorff, "Analysis of Reorientational Processes in Liquid Crystalline Side Chain Polymers Using Dielectric Relaxation, Electro-Optical Relaxation, and Switching Studies", Mol. Cryst. Liq. Cryst **177,** 13 (1989).

[100] H. Mensinger, M. Stamm, and C. Boeffel, "Order in Thin-Film of a Liquid-Crystalline Polymer", J. Chem. Phys. **96,** 3183–3190 (1997).

[101] I. Pelletier, I. Laurin, T. Buffeteau, B. Desbat, and M. Pézolet, "Infrared Study of the Molecular Orientation in Ultrathin Films of Behenic Acid Methyl Ester: Comparison between Single Langmuir-Blodgett Monolayers and Spin-Coated Multilayers", Langmuir **19,** 1189–1195 (2003).

[102] W. H. Kim, B. Bihari, R. Moody, N. B. Kodali, J. Kumar, and S. K. Tripathy, "Self-Assembled Spin-Coated and Bulk Films of a Novel Poly(Diacetylene) as Second-Order Nonlinear Optical Polymers", Macromolecules **28,** 642–647 (1995).

[103] T. Buffeteau, F. Lagugne-Labarthet, C. Sourisseau, S. Kostromine, and T. Bieringer, "Biaxial Orientation Induced in a Photoaddressable Azopolymer Thin Film As Evidenced by Polarized UV-Visible, Infrared, and Raman Spectra", Macromolecules **37,** 2880–2889 (2004).

[104] T.-Q. Nguyen, R. C. Kwong, M. E. Thompson, and B. J. Schwartz, "Improving the Performance of Conjugated Polymer-Based Devices by Control of Interchain Interactions and Polymer Film Morphology", Appl. Phys. Lett. **76,** 2454 (2000).

[105] S. Kirkpatrick, "Percolation and Conduction", Rev. Mod. Phys. **45,** 574–588 (1973).

[106] P. Dutta, B. Siswas, M. Ghosh, S. K. De, and S. Chatterjee, "The DC and AC Conductivity of Polyaniline-Polyvinyl Alcohol Blends", Synt. Met. **122,** 455–461 (2001).

[107] S. Strutz, S. Brower, and L. M. Hayden, "Temperature Dependence of the Activation Volume in a Nonlinear Optical Polymer: Evidence for Chromophore Reorientation Induced by Sub-T_G Relaxations", J. Pol. Sci. B **36,** 901–911 (1998).

[108] S. V. Novikov and A. V. Vannikov, "Field Dependence of Charge Mobility in Polymer Matrices", Chem. Phys. Lett. **182,** 598–602 (1991).

[109] K. R. Choudhury, J. G. Winiarz, M. Samoc, and P. N. Prasad, "Charge Carrier Mobility in an Organic-Inorganic Hybrid Nanocomposite", Appl. Phys. Lett. **82,** 406–408 (2003).

[110] D. M. Pai, "Transient Conductivity in Poly(N-Vinylcabazole)", J. Chem. Phys. **52,** 2285 (1970).

Acknowledgements

... and at the end, there is my gratitude.
The completion of this work has been, of course, only possible because of the help, assistance, and support from a number of people. It is my pleasure to pay due to them at least in the form of these words of acknowledgement.
I express my sincere gratitude to Prof. Karsten Buse. Not only has he given me the opportunity to pursue my Ph.D. through the University of Bonn, but he has also welcomed me in his group and opened many doors.
Special thanks go to Nils Benter and Ralph P. Bertram, who both have truly surprised me with how well we could work together, compensate each other's weaknesses, tease, mock in a nice way, and finally create an efficient teamwork that has been so much fun.
I thank Kim G. Jespersen and Christer Svanberg for at least temporally building up my small friendly *polymer* group in Denmark.
For their decisive contributions in fruitful collaborations, I want to thank Peter Sommer-Larsen for his assistance in dielectric spectroscopy, Wolfgang Hieringer for the density functional calculations, and Jens W. Andreasen for the X-ray scattering measurements.
My appreciation goes to the members of the Hertz group at the University of Bonn. I have felt at home during my stay and I have very much enjoyed the dynamics, nice atmosphere, and many discussions.
Furthermore, I thank my colleagues at the Risø National Laboratory who have contributed with various kinds of help, be it technical or organizational assistance or just answering a lot of my stupid questions.
Thanks go to Dr. Rainer Hagen and Dr. Serguei Kostromine from Bayer MaterialScience for providing the photoaddressable copolymers as well as tips and ideas.
Even though it might sound bizarre, I am serious about being thankful to the members of the Argentine tango community who helped me regularly recharging my batteries when the disordered materials would once more not behave as expected.
My thanks would not be complete if I did not mention my friends and family who have supported me along the way.
I am grateful to the Danish Research Council and the Deutsche Telekom AG for financial support.
Certainly, most of all, I have to express my deepest gratitude to Prof. Per Michael Johansen, not only for intensively supervising my Ph.D. project, but for being there whenever I needed him, with answers, council, encouragements, and actions. Also besides physics, I have learned so much. It was true a privilege to work with him.
It is with a humble heart that I acknowledge the breadth of perspective, knowledge, and experience that I have gained professionally, culturally, and personally. Thanks!
Dirk Apitz

List of own Publications

- **D. Apitz**, C. Svanberg, K. G. Jespersen, T. G. Pedersen, and P. M. Johansen, "Orientational Dynamics in Dye-Doped Organic Electro-Optic Materials", J. Appl. Phys. **94**, 6263-6268 (2003)
- **D. Apitz** and P. M. Johansen, "Limitations of the Stretched Exponential Function for Describing Dynamics in Disordered Solid Materials", J. Appl. Phys. **97**, 063507 (2005)
- R. P. Bertram, N. Benter, **D. Apitz**, E. Soergel, K. Buse, R. Hagen, and S. G. Kostromine, "Increased Thermal Stability of a Poled Polymer Using High-Molar-Mass Fractions", Phys. Rev. E, **70**, 041802 (2004)
- **D. Apitz**, R. P. Bertram, N. Benter, W. Hieringer, J. W. Andreasen, M. M. Nielsen, P. M. Johansen, and K. Buse, "Investigation of Chromophore-Chromophore Interactions by Electro-Optic Measurements, Linear Dichroism, X-Ray Scattering and Density-Functional Calculations", Phys. Rev. E, **72**, 036610 (2005)
- N. Benter, R. P. Bertram, **D. Apitz**, L. Bang Jacobsen, E. Soergel, P. M. Johansen, and K. Buse, "Large-Area Fabry-Pérot Modulator Based on Electro-Optic Polymers", Appl. Opt., **44**, 6235 (2005)
- **D. Apitz**, R. P. Bertram, N. Benter, P. Sommer-Larsen, P. M. Johansen, and K. Buse, "Conductivity of Oriented Bis-Azo Copolymer Films", Chem. Phys. Chem., (2005), in print.
- **D. Apitz**, "Transport Properties of Oriented Delocalized Hopping Sites - A Monte Carlo Simulation", (2005), in preparation.